CRITICAL SHEAR STRESS FOR EROSION OF FINE AND COARSE-GRAINED SEDIMENTS IN GEORGIA

A Thesis
Presented to
The Academic Faculty

by

Travis Harris

In Partial Fulfillment
of the Requirements for the Degree
Master of Science in the
School of Civil and Environmental Engineering

Georgia Institute of Technology
December 2015

CRITICAL SHEAR STRESS FOR EROSION OF FINE AND COARSE-GRAINED SEDIMENTS IN GEORGIA

Approved by:

Dr. Terry W. Sturm, Advisor
School of Civil and Environmental Engineering
Georgia Institute of Technology

Dr. Laurie A. Garrow
School of Civil and Environmental Engineering
Georgia Institute of Technology

Dr. Susan E. Burns
School of Civil and Environmental Engineering
Georgia Institute of Technology

Date Approved: December 2, 2015

ACKNOWLEDGEMENTS

I am grateful to my advisor, Dr. Terry Sturm, for his insightful support, his contagious desire for knowledge, and his leadership throughout this research. I would also like to thank Dr. Laurie Garrow for her relentless encouragement and invaluable comments. The feedback and guidance of Dr. Susan Burns are greatly appreciated. I also appreciate the time and interest of Dr. David Goldsman in this study. The laboratory work involved in this research would not have been possible without the diligent and knowledgeable work of Andy Udell, Blake Baklini, and Billy Plum. I am likewise thankful for the sediment donation from IMERYS. I would also like to thank the Georgia Department of Transportation (GDOT) for funding this project. A special appreciation is reserved for my family due to their support and unending encouragement. Finally I would like to give recognition to Marnie Williams for her care, prayer, and participation in every step along the way.

TABLE OF CONTENTS

LIST OF TABLES

LIST OF FIGURES

LIST OF SYMBOLS AND ABBREVIATIONS

$\bar{\tau}$	Average bed shear stress
ρ_b	Bulk density of sediments
ρ_w	Density of water
$\frac{\Delta D}{\Delta t}$	Displacement over time
ρ_{sand}	Dry density of fine sand
ρ_{kaolin}	Dry density of Georgia kaolinite
ρ_d	Dry density of sediments
m_{wet}	Mass of wet sediment
m_w	Pore water mass
$\hat{y}_i$	Predicted y-axis value
m_s	Solid mass of the sediment
V_t	Total unit volume
C_c	Coefficient of curvature
C_c	Coefficient of uniformity
CSF	Clay size fraction by weight
d_*	Dimensionless particle size
d_{10}	Particle size at which 10% of sediment by weight is smaller than
d_{30}	Particle size at which 30% of sediment by weight is smaller than
d_{50}	Median particle size
d_{50}	Particle size at which 50% of sediment by weight is smaller than

d_{60}	Particle size at which 60% of sediment by weight is smaller than
E	Erosion rate of sediment
Fr	Froude number
g	Gravitational acceleration
I_P	Plasticity index
$Kaolinite$	Kaolinite content by weight in decimal fraction
M	Experimental constant in linear-flux equation
n	Experimental constant in linear-flux equation
N	Number of data points
Q	Flow rate
R	Hydraulic radius of the channel
Re	Reynolds number
SE	Standard error of the estimate
SG	Specific Gravity
S_o	Bed slope of the channel
SSE	Summed square of the residuals
v	Kinematic viscosity of fluid
V	Mean flow velocity in an open channel
w	Water content
W_{LL}	Liquid limit
W_{PL}	Plastic limit
y	Flow depth
y_i	Measured y-axis value
y_o	Normal depth
γ	Sediment specific weight

γ_w	Specific weight of water
τ	Applied bed shear stress
τ_{*c}	Shields' parameter
τ_c	Critical shear stress
Fines	Percent of fines by weight
A	Activity of a sediment
r	Weight applied to equation
C_p	Mallows value
SSE_p	Sum of squares for evaluated model
MSE_{total}	Sum of squared error for model of all parameters
p	Number of parameters
n	Number of data points

SUMMARY

Erosion of a river bed has important implications with respect to scour around river structures such as bridges, transport of contaminants attached to the sediment, and disruption or destruction of aquatic habitats. Erosion occurs when the resistive strength of the sediment is overcome by the hydrodynamic forces produced by the flow of water. This resistance to erosion in a sediment originates from gravity or interparticle forces for coarse sediment (sand and gravel) and fine sediment (silt and clay), respectively. Since the erosion of fine sediment depends on the combination of many interparticle forces, and this combination fluctuates widely amongst different fine sediments, past studies have had difficulty finding a consistent method to estimate fine sediment erosion. This study analyzes sediments that fall in the transition size range between fine and coarse sediments and compares the findings with those from fine sediments (Wang 2013) and sandy coarse sediments (Navarro 2004, Hobson 2008), in order to correlate the erosion rates of both sediment types to their physical characteristics. In this study, kaolinite-sand mixtures were prepared by mixing various percentages of Georgia kaolinite by weight ranging from 30% to 100% with industrial fine sand and tap water. Geotechnical and other tests of sediment properties were performed to measure water content, bulk density, grain size distribution, temperature, pH, and conductivity of these mixtures. Hydraulic flume experiments measured the erosion rates of each sediment and these rates were used to estimate the critical shear stress correlating to that mixture. Relationships between the physical properties of the sediment and critical shear stress were developed by multiple regression analysis. An alternative option of estimating the critical shear stress by a

weighted equation, which uses the combination of fine sediment erosion and coarse sediment erosion equations separately, was explored and found to be a viable and accurate option to estimating both coarse and fine sediment erosion from the same parameters and equation. The results from this study can be used to estimate sediment erodibility and thus river bed stability based on simple tests of physical properties of the river bed sediment and will help predict scour around bridges and other flow obstructions.

CHAPTER I

INTRODUCTION

Erosion of sediment occurs naturally in river systems due to bed shear stresses produced by the turbulent flow of water over the river bed. Changes in the bed shear stress can come from flow around obstacles, turbulent flows along the bed, or flow changes that come from bends in the river. The amount of erosion that occurs normally can be dramatically increased around manmade structures due to the natural flow of the river being disturbed. Structures such as bridge piers, abutments, and bridge foundations cause river flow to contract and accelerate which causes higher bed shear stresses, flow separation, and increased turbulence in that area of the river. River beds around these structures experience complex flow patterns such as increased velocities, horseshoe vortices, and wake vortices. These complex flow patterns can lead to removal of sediments from the bed around the structures, which is known as scour. This scour, both from local scour and contraction scour, can jeopardize a bridge's foundation and has been found to be the primary cause of failure for bridge foundations and other hydraulic structures (Richardson and Davis 2001).

The hydrodynamic condition of the flow caused by the obstruction creates the possibility for erosion, but the properties of the bed sediment around these obstructions are what dictate the rate of erosion that occurs. Some sediments have a higher resistance to motion due to their physical properties and will not experience much scour. Other sediments may not be as resistant and much more scour might occur under similar conditions of bed shear stress and river flow. The submerged weight of particles is the dominant resistive force for coarse sediments such as sand and gravel. For the fine grained sediments (or "cohesive sediment"), it is the interparticle forces that mainly resist erosion, since the submerged weight of a fine sediment particle is negligible compared to the cohesive electrochemical forces between particles. Therefore in order to attempt to

predict or estimate the level of scour that will occur around certain hydraulic structures, the mineralogy of the sediment will need to be known in conjunction with the shear stresses produced at these locations.

Evaluating the total resisting force of sediments is difficult, especially for fine sediments. Currently the critical shear stress of fine sediments cannot be predicted accurately using geotechnical properties such as shear strength which was developed for designing weight-bearing structural foundations in residual sediments; thus, researchers have experimentally explored the relationship between critical shear stress and other sediment properties related to interparticle forces. The primary focus of this project is to build upon the erosion analysis of past research that relates sediment physical properties to a sediment's erodibility and produce a means to predict the critical shear stress for fine sediments based on these properties. Using Shelby tubes and a recirculating flume, Navarro (2004) studied the erosion of Shelby tube sediment samples from bridges throughout Georgia and related the erosion quantities found to the physical characteristics of percent fines and median grain size of the sediments. Hobson (2008) extended the work of Navarro using samples from five other Georgia bridges as well as relating the physical properties of these sediments to rheological properties of the fine particles in the sediments. Navarro and Hobson both tested the erodibility of mainly coarse sediments but also did experiments on sediments that crossed the threshold of fine and coarse. Wang studied the erosion of mixtures of Georgia kaolinite and ground silica using the same method as both Navarro and Hobson, and studied the rheological properties of these fine-grained mixtures as well. Wang correlated the clay size fraction in a sample and its water content to critical shear stress used in scour prediction equations. The current study links the work of Navarro, Hobson, and Wang by using mixtures of Georgia kaolinite and fine sand to bridge the gap between fine sediment data from Wang and coarser sediment data from Navarro and Hobson. This bridging of the gap between fine and coarse erosion data will produce an estimation of critical shear stress that can be used independently of

sediment size classification. The proposed prediction equation uses the cohesive characteristics of the sediment including water content and sediment size distributions to unify characterization of the erodibility of fine and coarse sediment.

The data from Navarro and Hobson, Wang, and the current study were combined to analyze the effectiveness of different equations on predicting both fine and coarse sediment erosion thresholds. Two main equation types were formed from the combination of these data sets; (1) a regression equation developed from all of the data which incorporated parameters from both equations developed by Wang (2013) and Hobson (2008); or (2) a weighted equation which applied a weighting factor to the two independent equations predicting fine sediment erosion or coarse sediment erosion, and added the contribution from both equations in order to predict the Shields parameter of a soil. The weighted equation, when compared to the regression equation, produced the most accurate results for both fine and coarse sediments and establishes one single equation that can correctly estimate the critical shear stress of fine or coarse sediment individually. This weighted equation eliminates the need to find a dividing line between fine or coarse sediment erosion equations and provides a great foundation for future studies to refine the accuracy of this equation.

The following chapter, Chapter II, contains a literature review of coarse and fine grained sediment erosion characteristics, erosion causes, erosion measurement methods, and kaolinite geology. Chapter III discusses the methods used in this experiment along with the materials used. Chapter IV includes the results of the experiments and the characterizations of the sediment mixtures. These results are analyzed and discussed in Chapter V. Lastly, the conclusions and recommendations for future research are made in Chapter VI.

CHAPTER II

LITERATURE REVIEW

2.1 Sediment Properties

The interactions between hydrodynamic forces and the strength of the sediments to resist erosion are what determine a sediment's stability in aquatic environments. Particle size of sediment is the primary factor affecting the sediment's resistance to erosion. Sediments fall into two different classifications based on their particle sizes. According to the American Geophysical Union (AGU) scale, sediments with particle diameters larger than 0.062 mm are classified as coarse sediments. Sediments with particle diameters smaller than 0.062 mm are called fine sediments and can be subdivided into silt and clay. Silt, a sediment classified by size in between sand and clay, has a particle size range from 0.002 mm to 0.062 mm. Clay-sized particles are smaller than 0.002 mm. Coarse, non-cohesive sediment erosion and transport have been extensively studied in both laboratory and field studies. These experiments show that gravity acting on each particle in the form of its submerged weight is the main force in a coarse sediment's resistance to erosion. Fine sediments (or sediments made up of both silt and clay) have a resistance that comes from interparticle forces including physical properties of the sediments, electrochemical reactions, consolidation, and biostabilization (Stone et al. 2011). Fine sediments have different erosion resistance factors than coarse sediments, indicating that erodibility and transport mechanisms differ for coarse and fine sediments. Therefore, it is not appropriate to estimate fine sediment erosion by extrapolating from equations developed using coarse sediment erosion data.

The erosion of fine sediments is important in rivers, estuaries, and aquatic environments. These sediments are referred to as "mud", cohesive sediment, or fine-grained sediment in research relating to estuaries, hydraulic studies of rivers, or geotechnical fields, respectively. Ecologically, fine-grained sediments are habitats for

benthic organisms, stores for organic carbon, and sites of biological cycling (Grabowski et al. 2011). When erosion and transport of these fine sediments do occur, it can be harmful to downstream environments and harm the environments the sediments were eroded from. The erodibility, or propensity for the sediment to be eroded, of cohesive sediment is influenced by a range of physical, geochemical and biological sediment properties and processes; these include particle size distribution, bulk density, water content, temperature, clay mineralogy, total salinity, relative cation concentrations, pH, metal concentrations, bioturbation, and biogenic substances, and particularly extracellular polymeric substances or EPS (Grabowski et al. 2011).

The large number of properties that affect sediment erosion and their interactions have been one of the main reasons that an empirical relationship for all cohesive sediment erosion has not been found. The difficulty involved with analyzing all of these factors simultaneously has led many researchers to analyze a subset of factors that they believed to be most responsible for the variation in erodibility in their particular sediments. Some of these studies have taken the amount of fines (silt and clay content in a sediment) in the sediment as the primary factor for fine sediment erosion. These are typically studies that used mixtures made in the laboratory. Other studies have focused on the clay content instead of the silt and clay content because it is the clay content within the mud that provides the interparticle cohesion (van Ledden et al. 2004). It is important to distinguish the difference between clay and silt because of the impact their differing particle size has on mineralogy, water confinement capability, and electrochemistry at the particle surface (Santamarina et al. 2001, Wang 2013). Clay particles, due to their flat plate-like structure which produces a large overall surface area in the sediment, have a high capability to hold water, whereas the larger silt particles have less surface area and less surface reactivity.

Some investigators have used bulk density and water content together as primary indicators of the variation in erosion since these two factors are related measures of the

solid and liquid states in the sediment under the assumption of fully saturated sediment (Rowell 1994; Avnimelech et al. 2001). These two characteristics' role in cohesive sediment erodibility has been extensively studied in both field and laboratory studies. According to Grabowski et al. (2011), "bulk density is the principal source of variation in erodibility by depth in natural cohesive sediment." Water content, however, cannot be disregarded because it is an important factor which affects the erodibility of a cohesive sediment (Thoman and Niezgoda 2008), and it can be calculated from bulk density for saturated sediments.

2.2 Causes of Erosion and Various Types

Erosion occurs in sediment when the erosional forces from the flow of water are greater than the resistance forces of the sediment. In coarse sediments, this occurs when the gravity force of the individual particle is overcome by the bed shear stress, or the drag force per unit area. Coarse sediment erosion is widely understood and several models exist that accurately predict coarse sediment erosion in rivers (Sturm 2010). In contrast, fine sediment erosion occurs when the flow forces are greater than the combination of interparticle forces in an individual particle or in a group of particles. The capability to predict fine sediment erosion is still in question (Grabowski 2011). For either coarse or fine sediment, the threshold for particle movement is defined as the critical shear stress, τ_c. Critical shear stress is the value of the bed shear stress at which the hydrodynamic forces overcome the resistive forces of sediments and movement of sediment particles begins. Erosion of sediment increasingly occurs at shear stresses higher than this value, proportionally to the increase of bed shear stress.

Erosion refers to the net loss of sediment particles from a specific area and there are multiple forms in which it can occur. Four forms of erosion are identified in the literature and include entrainment, mass erosion, surface erosion, and floc erosion (Winterwerp and Van Kesteren 2004, Mehta 1991, Partheniades 1965). Entrainment is

defined as fluid mud being entrained by a turbulent flow. When larger clumps of sediment are eroded along an entire plane below the surface of the sediment, typically due to high shear stresses, this is defined as mass erosion. Surface erosion occurs when small flocs and aggregates are carried downstream after the hydrodynamic forces have overcome the interparticle forces. Surface erosion occurs at low to medium bed shear stresses; the rate of erosion increases with an increase in the bed shear stress and is common in rivers and estuaries (Mehta et al. 1988). Floc erosion is the removal of individual flocs of sediment from the bed due to a peak turbulent bed shear stress, when the average bed shear stress, $\bar{\tau}$, is less than the average bed drained strength, or critical shear stress, τ_c. (Jacobs 2011). A relationship for the transitions between these erosion modes has been defined as follows: $0.5\ \tau_c > \bar{\tau}$, stable bed; $0.5\ \tau_c < \bar{\tau} < \tau_c$, floc erosion; $\tau_c < \bar{\tau} < 1.7\ \tau_c$, floc and surface erosion; and $\bar{\tau} > 1.7\ \tau_c$, surface erosion (Winterwerp et al., 2012).

Another method to categorize erosion is based on the time dependency of the erosion rate as developed by Mehta and Partheniades (1982). Type I, or time-dependent erosion, is defined by a decreasing erosion rate with time under a constant bed shear stress. Time dependent erosion can be due to the stratification of the sediment bed as density and critical shear stress increase with depth. Type I erosion can also be subdivided into (Type 1a) erosion of surficial fluff and (Type 1b) erosion of the underlying bed (Amos et al. 1997). Homogenous beds with consistent size distribution and density over depth have an erosion rate that remains constant over time with a constant bed shear stress. This is denoted as Type II erosion and operates under the assumption that critical shear stress and density are constant throughout the depth.

Critical shear stress, τ_c, is defined as the applied bed shear stress at which erosion begins. As discussed previously, erosion can happen at an applied bed shear stress that is less than the critical shear stress, but is assumed negligible (Osman and Throne 1988; Hanson 1990; Karmaker and Dutta 2011). Erosion that occurs at bed shear stress less

than the erosion threshold can be explained by the recognition of time-decreasing (Type I) and time-independent (Type II) erosion (Jacobs 2011). In this study, critical shear stress is defined as the applied bed shear stress at which surface erosion occurred. For bed shear stresses less than this where floc erosion did occur, erosion was assumed negligible. This method coincides with that used by Jacobs (2011), in which critical shear stress is defined as the onset of transport of both sand and mud, not the threshold for the initiation of motion of either.

2.3 Erosion Rate Measurement Devices and Equations

In order to estimate sediment erosion properties, devices have been developed to measure sediment erodibility of both laboratory and field samples. Laboratory flumes, benthic in situ flumes, and submerged jets are the three main devices used. Laboratory flumes are used on both field samples and samples made in the laboratory by artificially mixing sediments of differing size and mineralogy. These flumes can be straight or rotating annular flumes, and are typically recirculating. Benthic in situ flumes are used in the field to measure erodibility of sediments in their natural environment. These flumes measure bed shear stresses in natural rivers, lakes, wetlands, bays, harbors, and estuaries. Benthic in situ flumes can be classified as recirculating flumes or straight flow-through flumes, but both methods correlate the Suspended Sediment Concentration (SSC) to flow rates that come from specific hydrodynamic conditions. Submerged impinging jets, commonly known as Cohesive Strength Meters (CSM), are used widely in the field since they are portable. The method of measurement consists of eroding sediment using a jet that is directed perpendicular to the plane of the sediment. Short bursts of pressurized water erode the sediment which then mixes with the water in the container area of the device. The transmission of light through the sediment water slurry is then measured. This allows for calculations of both erosion rates and the resettling rates of the sediment. Examples of studies using these measurement devices are shown in Table 2.1.

Table 2.1: Examples of Erosion measurements devices

Type			Sample Source	Author(s)
Applied in	Flume Shape	Device Name		
Laboratory	Straight, recirculating flume	-	Kaolinite; river samples	Dennett (1995)
		Sedflume	Undisturbed samples from Riverbeds	McNeil et al. (1996)
			Reconstructed samples from riverbeds	Jepsen et al. (1997)
			Quartz particles	Roberts et al. (1998)
			Undisturbed and reconstructed samples from field; Pure clay (Kaolinite, Bentonite); Quartz particles	Lick and McNeil (2001)
		ASSET	Quartz particles	Roberts et al. (2003)
		-	Georgia kaolinite	Ravisangar et al. (2001, 2005)
		-	Sand and clay mixture	Barry et al. (2006)
		-	Undisturbed samples from riverbed and coastal area	Ganaoui et al. (2007)
		-	Undisturbed samples from lakes	Rightti and Lucarelli (2007)
		-	Undisturbed samples from riverbeds	Ternat et al. (2008)
	Straight, recirculating duct	EFA	Silt and clay mixture; Kaolinite	Briaud et al. (1999, 2001, 2004)
	Rotating annular flume	-	Boston Blue Clay	Zreik et al. (1998)
		-	Sand and clay mixture	Jiang et al. (2004)
Field	Submerged impinging jet	-	Mixture of clay (40%), silt (53%), and fine sand (7%)	Mazurek et al. (2001)
		-	Sand and clay mixture	Ansari et al. (2003)
	Benthic recirculating flume	Sea Carousel	Bay of Fundy, Canada	Amos et al. (1992a, b)
		VIMS Sea Carousel	Chesapeake Bay and Middle Atlantic Bight	Maa et al. (1993)
			Baltimore Harbor	Sanford and Maa (2001)
		-	Humber estuary, U.K.	Widdows et al. (1998)
	Benthic recirculating race-track shaped flume	MORF	South Wales, U.K.	Black and Cramp (1995)

(Table 2.1 Continued)

	Benthic vertical recirculating flume	ISEF	Dutch Wadden Sea coast	Houwing and van Rijn (1998); Houwing (1999)
	Benthic flow-through flume	Seaflume	Buzzards Bay, Mass	Young (1977)
			Puget Sound Basin	Gust and Morris (1989)
		-	Boston Harbor	Ravens and Gschwend (1999)
		NIWA I, II	Several rivers, wetlands, and lakes	Aberle et al. (2003, 2003, 2006); Debnath et al. (2007)
	Submerged impinging jet	CSM	Severn estuary, U.K.	Paterson (1989)
		modified CSM	Sylt mudflat, Germany	Tolhurst et al. (1999)
			Tollesbury, Essex, U.K.	Watts et al. (2003)
		-	Urbanizing basin near Toronto, Canada	Shugar et al. (2007)
	Circular inverted bell-shaped funnel	ISIS	Severn estuary, U.K.	Williamson and Ockenden (1996)

Source: Wang (2013) Table 2.2

In addition to the existence of many devices that have been used to measure erosion rate and erosion threshold, there are multiple forms of mathematical expressions that have been applied to predict these erosion rates for cohesive sediments. Some of the expressions are found in Table 2.2 along with a description of each variable. The majority of these equations incorporate bed shear stress, density, and critical shear stress in order to predict the erosion rate. Often the goal of laboratory studies is to measure the critical shear stress parameter which appears in several of the expressions. The most common form of expression relates erosion rate E to applied shear stress τ with the experimental sediment erodibility parameters of M, n, and τ_c. The equation used in this study, the excess shear stress-flux equation, can be expressed as:

$$E = M(\tau - \tau_c)^n \tag{2.1}$$

where E = erosion rate (kg/m^3/s); τ = applied bed shear stress (Pa); τ_c = critical shear stress (Pa); and M and n are experimental constants. The variables E, M, n, and τ_c in Eq. (2.1) all depend on the applied bed shear stress and all describe the sediment's resistance to erosion based on the physical properties of the sediment at that bed shear stress (Grabowski 2011; Winterwerp and van Kesteren 2004; Mehta et al. 1988). This equation has been applied to both coarse grained sediments and fine grained sediments in past studies. To simplify the equation some studies have set n = 1, to describe Type II erosion which has a constant τ_c over depth. This study focuses on erosion rates in a stratified sediment bed after settling and therefore includes n as an erosion parameter that is not equal for all depths. This nonlinear erosion behavior is exhibited in many examples of sediments with cohesive erosion characteristics (Walder 2015).

Table 2.2: Mathematical expressions for cohesive sediment erosion

Investigator(s)	Expression	Note
Ariathurai (1974)	$E = M(\tau - \tau_c)$	E : erosion rate ($kg/m^2/s$) τ : bed shear stress (N/m^2) τ_c : critical shear stress, value of τ as $E \approx 0$ (N/m^2) M, n : experimental constant
Lick (1982) and others	$E = M(\tau - \tau_c)^n$	
Kandiah (1974)	$E = M\left(\frac{\tau}{\tau_c} - 1\right)$	
Mehta (1991)	$E = M\left(\frac{\tau - \tau_c}{\tau_c}\right)$	
Gularte et al. (1980) and others	$E = \varepsilon_f \exp\left[\alpha(\tau - \tau_c)^\beta\right]$	E : erosion rate ($kg/m^2/s$) τ : bed shear stress (N/m^2) τ_c : critical shear stress, value of τ as E ≈ 0 (N/m^2) ε_f : the flow erosion rate when τ-τc = 0, no mean flow velocity dependent surface erosion by definition; empirically determined. α, β : experimental constants β = 0.5 reported by Parchure and Mehta (1985)
Roberts et al. (1998)	$e = A\tau^n \rho_b^m$ Define: $\tau_c = \left(\frac{e}{A}\right)^{1/n} \rho_b^{-m/n}$ @ $e = 10^{-4}$ (cm/s)	e : volumetric erosion rate (cm/s) τ : bed shear stress (N/m^2) ρ_b : bulk density (g/cm^3) A, n, m, c, k : experimental constants
	$e = c\tau^n \exp(-k\rho_b)$	
Bruid et al. (1999)	$e = \left(\frac{5.54\tau - 2.77}{\tau + 0.875}\right) + 0.178\tau - 0.0809$ $\tau_{\max} = 0.094\rho_w V^2 \left(\frac{1}{\log \mathrm{Re}} - \frac{1}{10}\right)$ $e = e_i \ @ \ \tau = \tau_{\max}$ $z_{\max} = 0.18\,\mathrm{Re}^{0.635}$ $z = \frac{t}{\frac{1}{e_i} + \frac{t}{z_{\max}}}$	e : scour rate (mm/hr) τ : bed shear stress (N/m^2) ρ_w : density of water (kg/m^3) V : mean flow velocity $Re = \frac{VD}{v}$; D : pier diameter, v: kinematic viscosity of water e_i (mm/hr) : erosion rate at τ_{max} z : scour depth (mm) after a period of scour developing time, t (hr)

(Table 2.2 Continued)

Krone (1999)	$E = a_0 + a_1\rho_b$ where $a_i = b_{2i}\tau^2$ $\Rightarrow E = b_{20}\tau^2 + b_{21}\tau^2\rho_b$	E : mass erosion rate ($kg/m^2/s$) or ($g/cm^2/s$) τ : bed shear stress (N/m^2) or ($dynes/cm^2$) bulk density (kg/m^3) or (g/cm^3) b_{2i} : experimental constants
	$E = K_2(\rho_{\max} - \rho_b)\tau^2$, $\rho_b < \rho_{\max}$ Dimensional considerations: $E = \frac{k}{\mu g}\frac{(\rho_{\max} - \rho_b)}{(\rho_s - \rho_w)}\tau^2$	ρ_{max} : the maximum bulk density that can be reached before the sediment structure becomes denser; can be define from the plot of E vs. ρ_b ρ_s : density of particle (kg/m^3) or (g/cm^3) ρ_w : density of water (kg/m^3) or (g/cm^3) μ : viscosity of water ($N*s/m^2$) g : acceleration of gravity (m/s^2) K_2 : experimental constant k : dimensionless structure constant
Sanford and Maa (2001)	$E = \rho_b\beta(\tau - \tau_{c0})\exp[-\gamma\beta(t - t_0)]$	E : erosion rate ($kg/m^2/s$) ρ_b : bulk density (kg/m^3) τ : bed shear stress (N/m^2) τ_c : critical shear stress $\gamma = \frac{d\tau_c}{dt}$ t_0 : time at which a new stress level is applied τ_{c0} : the value of τ_c evaluated at $t = t_0$ β : local constant

Source: Wang (2013) Table 2.3

2.4 Kaolinite Geology and Mineralogy

The fine-grained sediment employed in this study to create sediment mixtures was Georgia sedimentary kaolinite which is an industrial mineral widely used in paper as a filling and coating pigment. Georgia kaolinite is also incorporated into rubbers, plastics, paints, and ceramics. Volume, purity, and diversity are some of the physical properties that set Georgia kaolinite apart from other kaolinites found elsewhere in the world.

Georgia kaolinite is classified as a fine sediment with particles in both the clay and silt ranges. Georgia kaolinite has two categories based on the age and size of the sediment. Younger "hard" kaolinites are from the Paleocene-Eocene time period and more than 80% of their particles are smaller than 0.002 mm by weight. The older, "soft", kaolinite from Cretaceous periods contain layered stacks of kaolinite particles and more than 70% of their particles are larger than 0.002 mm (Pruett 2000). The kaolinite used in this study is an older "soft" kaolinite. Past studies have been dedicated to characterizing the particle geometry and mineral content of Georgia kaolinite deposits (Bundy et al. 1965; Brindley 1986).

Three of the main groups of clay minerals that are separated by their electro-chemical activity and size are kaolinites, micas, and smectites (Partheniades 2007). Of these, kaolinites are the least electro-chemically active mineral due to having the largest particles and lowest cation exchange capacity (CEC) of the three. These three groups are all fine, clayey sediments, but each group affects sediments in different ways by producing varying amounts of water content capacity, different erosion thresholds for the same amount of clay by weight, as well as diverse reactions to biological influences. Montmorillonite, a smectite, when mixed with sand has been found to produce a lower critical shear stress than either kaolinite or natural marine mud (Torfs 1996). The different types of clays, which have dissimilar surface areas, require distinct amounts of wetting to move a sediment from solid behavior, liquid behavior, or plastic behavior and into another behavior phase. The activity, or ratio of plasticity index to percent of clay sized particles by weight, helps to differentiate between the various types of clay. A specific clay activity is a good representation of the effect that a clay type has on the sediment structure and water content capacity.

The structure of kaolinite sediments also depends on the electro-chemical forces between particles. Kaolinites are two-layer type crystals which have sheet structures made up of a layer of alumina octahedrons and another layer of silica tetrahedrons (Velde

1995; Murray 2007). Cohesive strength is often determined by the amount of fine sediment in a sediment, and this strength has been considered more important than the packing density in the past (Jacobs 2011).

The structure of clay in kaolinite sediment is an important parameter relating to the erosional stability of a cohesive sediment. Three different particles associations are found to occur during settling of a clay suspension. These are edge-to-face (E-F), edge-to-edge (E-E), and face-to-face (F-F). Flocculated suspensions for kaolinite, which typically occur for pH less than 5.5, have predominately E-F associations and exhibit a strong stratification with respect to erosional strength throughout the depth. High pH and low ionic strength produce F-F associations which have less erosional strength stratification but strong stratification in bulk density with respect to depth. The bed stability of kaolinite sediment is related to the initial suspension characteristics. The erosional stability is therefore related to the particle associations and the stratification of this erosion is highly dependent on the type of associations formed from settling sediment.

2.5 Findings of Previous Research

Navarro (2004) and Hobson (2008) both experimented on coarse field samples from bridges around Georgia to find a connection between the critical shear stress and the physical properties of the field sediments. The Shields parameter, τ_{*c}, is a dimensionless variable used to describe incipient sediment motion. This parameter is the ratio of applied bed shear stress to the gravitation force per unit volume at critical conditions and is calculated by (Shields 1936):

$$\tau_{*c} = \frac{\tau_c}{(\gamma_s - \gamma) d_{50}} \tag{2.2}$$

$$d_* = \left[\frac{(SG-1) g d_{50}^3}{\nu^2} \right]^{1/3} \tag{2.3}$$

with the dimensionless diameter's calculation in Eq. (2.3). Shields provides an accepted, well established experimental relationship between τ_c and d_* which was based off of the results from many investigators. This relationship was created from sand and gravel data.

Hobson combined his data and that of Navarro to produce Eq. (2.4) which relates the Shields parameter to the percent of fines in the sediment by weight, and the dimensionless diameter. Only the percent of fines, *Fines*, were necessary in the equation to establish a good fit to the data but he included the dimensionless diameter in order to include the viscous influence of the flow on the erosion process. This equation estimates the dimensionless erosion for coarse sediment and is limited to coarse sediments as it poorly estimates the Shields parameter for fine sediments since there is no inclusion of the cohesiveness provided by the clay.

$$\hat{\tau}_{*_c} = 0.644 \times 10^{2.68 Fines} d_*^{-0.409} \tag{2.4}$$

Wang (2013) experimented on laboratory mixtures of silt and kaolinite which are fine sediments with clay size fractions ranging from 3% to 30%. She also correlated physical properties of the sediment to the Shields parameter but based her equation off of a combination of the water content, *w*, and clay size fraction, *CSF*, of the sediment. Her equation, Eq. (2.5), is limited to predicting the Shields parameter for sediments with a median particle size less than 0.1mm and is therefore not as good of a predictor of coarse sediment erosion.

$$\hat{\tau}_{*_c} = 8.46 - 27.76w + 73.69CSF + 83.22(w \times CSF) \tag{2.5}$$

This study will use new erosion data of sand and kaolinite mixtures in conjunction with the data from all three of these studies to identify an erosion estimation relationship that will allow for the prediction of critical shear stress for both coarse and fine sediment.

2.6 Summary of Literature Review

This chapter discussed the differences in coarse and fine sediment resistance to erosion. Fine sediment erosion rates are controlled by interparticle forces, not gravity, and are dependent on many factors. Many of these factors have been individually examined through experiments and their relationships with sediment erosion rate have been analyzed. Of these factors, the water content and geotechnical characterizations related to the median size and size distribution of the sediment have been identified as primary variables in determining sediment erodibility. Out of the four modes of erosion identified in the literature, surface and floc erosion are the two that occurred in this study and the distinction between the two is an important concept in defining the erosion threshold. This research builds off of three studies that explored erosion rates of coarse-grained and fine-grained sediments (Navarro 2004; Hobson 2008; Wang 2013). The sediment mixtures created and tested in this study are in the transition size range from fine to coarse and we will develop a method of estimating erosion rates for sediments that have both fine and coarse characteristics. Past studies have shown that it is not accurate to extrapolate from coarse sediment erosion data to estimate fine sediment erosion, but the current study will analyze the sediments in between in order to more fully understand the physical properties affecting erodibility of fine and coarse sediments. The next chapter will discuss the methods and materials used to examine these sediments.

CHAPTER III

EXPERIMENT SETUP AND PROCEDURE

This chapter covers the procedure implemented before, during, and after each erosion test. Included are methods for measuring grain size distribution, Atterberg values, water content, bulk density, pH, conductivity, and temperature of the sediment slurry. Also discussed are the materials and equipment used during the erosion tests in the hydraulic flume. This section will explain the steps taken to ensure that all experiments were completed in identical manners in order to ensure that the final data are consistent and that experimental error has been minimized.

3.1 Sediment Preparation and Classification

Two types of sediment materials were used in the preparation of specimens for this study; Georgia kaolinite (Kaolin) and fine industrial sand. The Georgia kaolinite was obtained from IMERYS, with Georgia headquarters located in Roswell, Georgia. It is mined in middle Georgia near Dry Branch, GA and graded as Hydrite Flat DS. This kaolinite is wet processed and the size distribution is measured and checked using the Sedigraph technique. The Georgia Kaolin is made up of 95% kaolinite with small amounts of mica that vary from batch to batch and is dependent on the natural amount of mica within the crude source of kaolinite. No additives are used in the processing of Hydrite Flat DS. The fine sand was purchased from Surface Prep Supply in Haines City, FL. The fine sand is manufactured by Standard Sand and Silica and is graded between the #70 and #200 sieves. The fine sand has a median diameter particle of 0.122 mm and a specific gravity of 2.65. Table 3.1 displays physical properties of each sediment.

Table 3.1: Physical properties of kaolinite component in experimental mixtures.

Property	Units	Value
d_{50} from hydrometer	(micron)	3.3
d_{50} from Sedigraph	(micron)	4.0
Brightness	(GE% of MgO)	81.5
pH	(20% Solids)	4.7
Residue on 325 Mesh Screen	(wt. %)	0.25
Oil Absorption	(%)	34
Surface Area	(B.E.T. Nitrogen - m2/g)	7

Four mixtures of these two sediments were used in these experiments in order to investigate how the variation in sediment properties affects critical shear stress. The procedure for mixing the two sediments involved including enough water to guarantee full saturation of the sediment. This ratio of sediment to water was 15 g of sediments to 20 ml of water which provided consistent water content values at similar depths for each identical mixture and also allowed the full volume of any wet mixture to fit inside the Shelby tube container for settling. An electronic blender was used to fully disperse and mix the combination of the kaolinite, fine sand, and water. After mixing, the mixture was then poured into a cut-off section of a Shelby tube. Five of these tubes were used, all having an inner diameter of 72.8 mm, outer diameter of 76.2 mm, and average height of 290 mm. The sediment mixture was allowed to settle in the tube with a piston head acting as the bottom of the container for 24 hours. This 24 hour period was found to be an adequate time for full sedimentation to occur (Wang 2013). After 24 hours, excess water on the surface of the specimen was suctioned off, and care was taken not to disturb the sediment specimen. Then the tube was inserted into the bottom of the flume. Table 3.2 shows the mixtures of fine sand and kaolinite used in this experiment and their corresponding percent of the total mass.

Table 3.2: Mixtures of Georgia kaolinite and fine sand

Percent by weight of sediments	Fine Sand		Georgia Kaolinite		Total Air-Dry Weight (g)
	Air-dry weight (g)	Percent of total mass %	Air-dry weight (g)	Percent of total mass %	
0% K - 100% S	600	100%	0	0%	600
30% K - 70% S	420	70%	180	30%	600
50% K - 50% S	300	50%	300	50%	600
70% K - 30% S	180	30%	420	70%	600
80% K - 20% S	120	20%	480	80%	600
100% K - 0% S	0	0%	600	100%	600

3.2 Characteristics of the Sediment

Sediment characterization techniques were used to measure the following sediment properties for each mixture: grain size distribution, water content, dry and bulk densities, and Atterberg limits. In addition, the temperature, pH, and conductivity of the sediment and water slurry were measured immediately after mixing.

Grain size distributions were obtained using sieve analysis methods and hydrometer tests. The fine sand was dry sieved in accordance with ASTM C136-01 (ASTM International 2001). The Georgia Kaolinite was analyzed using a hydrometer test with a 151H hydrometer and by following ASTM D422-63 (ASTM International 2002). For the fine sand, sieves with mesh openings of 0.250 mm (#40), 0.210 mm (#70), 0.150 mm (#100), 0.106 mm (#140), 0.075 mm (#200), 0.063 mm (#230), and 0.053 mm (#270) were used. Both of these grain size distribution curves are plotted in Figure 3.1. These curves were used to determine the median particle size (d_{50}) by estimating the value of the particle size on the curve where the curve crosses the 50% finer line.

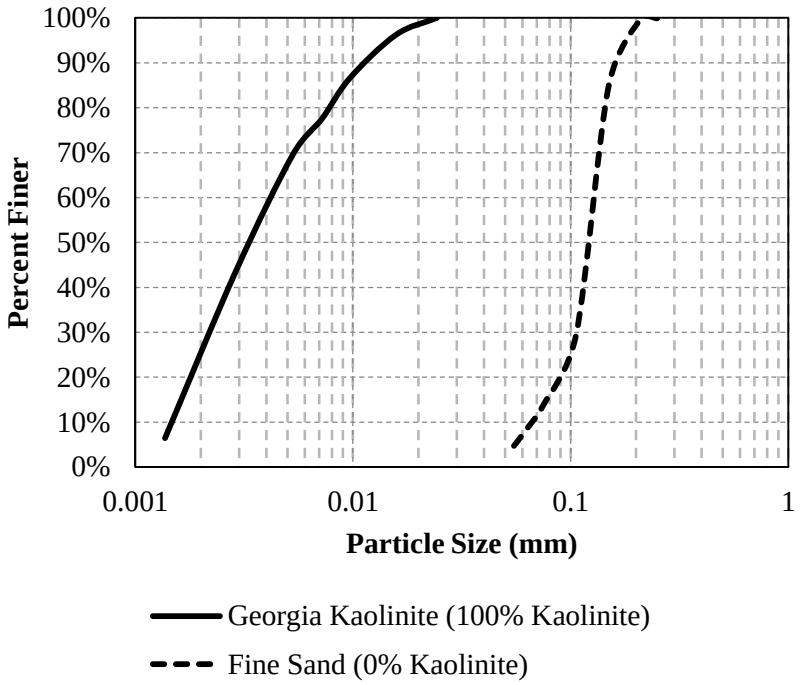

Figure 3.1: Size distributions of Georgia kaolinite and fine sand

In order to characterize the general plasticity properties of the fine-grained sediment mixtures, Atterberg limits were measured. The following Atterberg values were used in this study: liquid limit, plastic limit, and plasticity index. The relationship of these three values is shown below according to ASTM D4318 – 10 (ASTM International 2010b).

$$I_P = w_{LL} - w_{PL} \tag{3.1}$$

The plasticity index, I_P, which gives the range of water content over which a sediment behaves plastically, is determined as the difference between the liquid limit (w_{LL}, lower limit of viscous flow) and the plastic limit (w_{PL}, the lower limit of the plastic state) (Holtz and Kovacs 1981). These Atterberg values are used to show where the boundaries between the liquid and solid phases are located for a specific sediment. The

liquid limit and plastic limit are both water content values at which the respective liquid or plastic conditions occur at for that sediment. A water content higher than the liquid limit correlates to a sediment that behaves similarly to a liquid. The range of possible plasticity index values is categorized as highly plastic for $I_p > 17$, medium plastic for $17 \geq I_p \geq 7$, low plastic for $7 \geq I_p$, and non-plastic for $I_p = 0$ (Ranjan and Rao 2000).

Water content (w) measurements were also taken for each sediment. Water content measurements consist of measuring the weight of the specimen before and after drying using an electronic balance and following ASTM D2216-10 (ASTM International 2010a). Water content is the ratio of pore water mass (m_w) to solid mass of the sediment (m_s). This ratio was used to calculate both the bulk density (ρ_b) and dry density (ρ_d), defined as the ratio of wet sediment or dry sediment per total unit volume (V_t) respectively.

$$w = \frac{m_{wet} - m_s}{m_s} = \frac{m_w}{m_s} \tag{3.2}$$

$$\rho_d = \frac{m_s}{V_t} \tag{3.3}$$

$$\rho_b = \frac{m_{wet}}{V_t} \tag{3.4}$$

The water content was used to estimate the bulk and dry densities by assuming that the specimens were fully saturated. This assumption is made possible by using enough water in the mixing procedure so that all pore spaces can be completely filled with water. The equations shown below are used to estimate bulk and dry density from the water content, since the total volume is made up of only water and sediment when the specimen is fully saturated.

$$\rho_d(w) = \frac{m_s}{V_t(w)} = \frac{m_s}{\frac{w \times m_s}{\rho_w} + \left[\frac{m_s \times (1 - Kaolin)}{\rho_{sand}} + \frac{m_s \times Kaolin}{\rho_{Kaolin}}\right]} \tag{3.5}$$

$$\rho_b(w) = \frac{m_s}{V_t(w)} = \frac{m_{wet}}{\frac{w * m_s}{\rho_w} + \left[\frac{m_s * (1 - Kaolin)}{\rho_{sand}} + \frac{m_s * Kaolin}{\rho_{Kaolin}}\right]} \tag{3.6}$$

The last group of characteristics measured included temperature, pH, and conductivity of the water and sediment slurry immediately after dispersion with the blender and before the 24 hour settling period began. These measurements were done with the Oakton Waterproof PC 300 Meter. Conductivity and pH calibrations were performed before any experiments were conducted, and the temperature was calibrated by the manufacturer.

3.3 Experimental Procedure for the Hydraulic Flume

Experiments for this study were performed in the Hydraulics Laboratory in the School of Civil and Environmental Engineering at Georgia Institute of Technology. The flume used is a recirculating, rectangular, tilting flume measuring 6.1 m long and 0.38 m both deep and wide. A 1.9 m^3 storage tank holds the water recirculated through the flume and a variable-speed 6–in. slurry pump that can pass large solids transports the water from the tank at the end of the flume to the beginning of the flume. In the flume is a bed of fixed gravel with d_{50} = 3.3 mm which ensures that the flow is in fully rough, turbulent condition at the specimen location during the erosion test (Hobson 2008). The specimen is inserted into a hole made for the Shelby tube, and a hydraulic jack inserted into the bottom of the piston head extrudes the sediment into the flow of the flume.

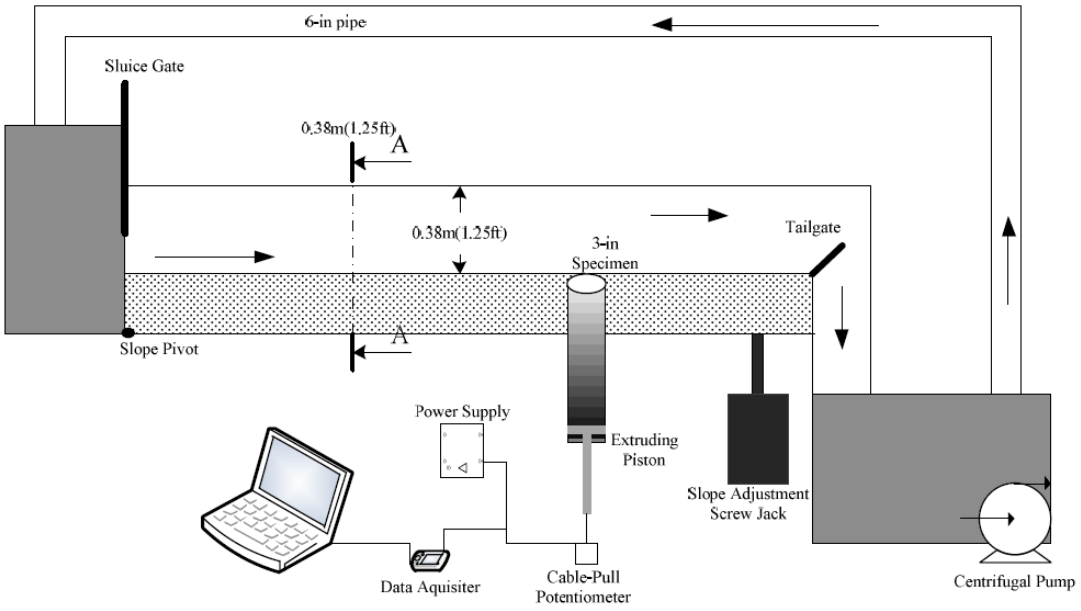

(NOT TO SCALE)

Figure 3.2: Flume apparatus for erosion tests

Source: Wang (2013) Figure 3.7

Figure 3.3: Photo of flume, storage tank, and other experiment equipment

To adjust the flume to a desired bed shear stress (τ), the flow rate (Q), flow depth (y_o), and slope (S_o) can be set at predetermined values. First, the slope is positioned using the calibration equation for the slope counter and flume jack located at the downstream end of the flume with the pivot at the upstream end (Ravisangar et al. 2001). Then the flow rate is established using the relationship calibrated between the manometer deflection of the bend meter and the flow rate (Hoepner 2001). These two calibration equations are given in Figure 3.4 and Figure 3.5.

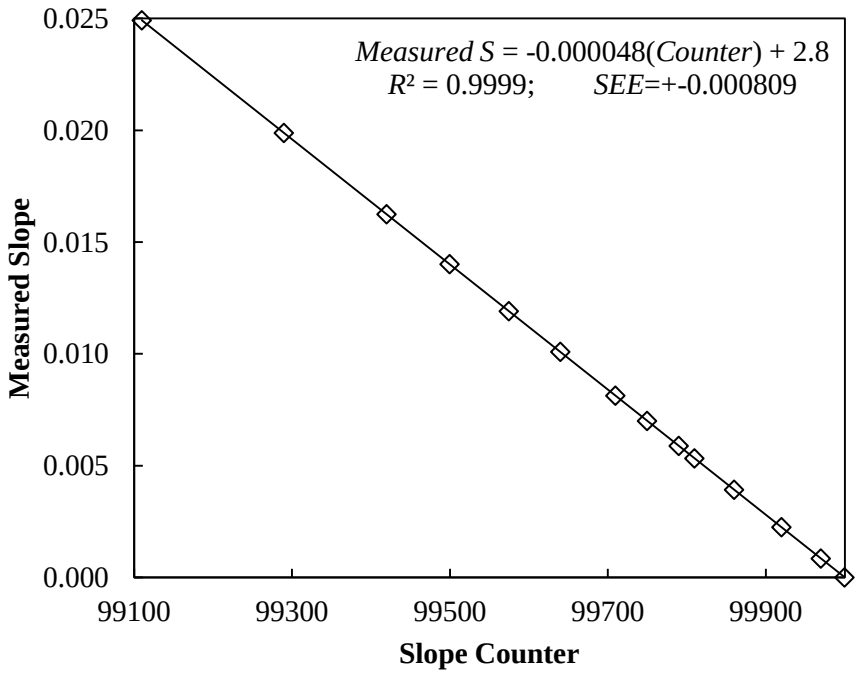

Figure 3.4: Calibration of flume slope counter and slope

Source: adapted from Navarro (2004) Figure 3-6

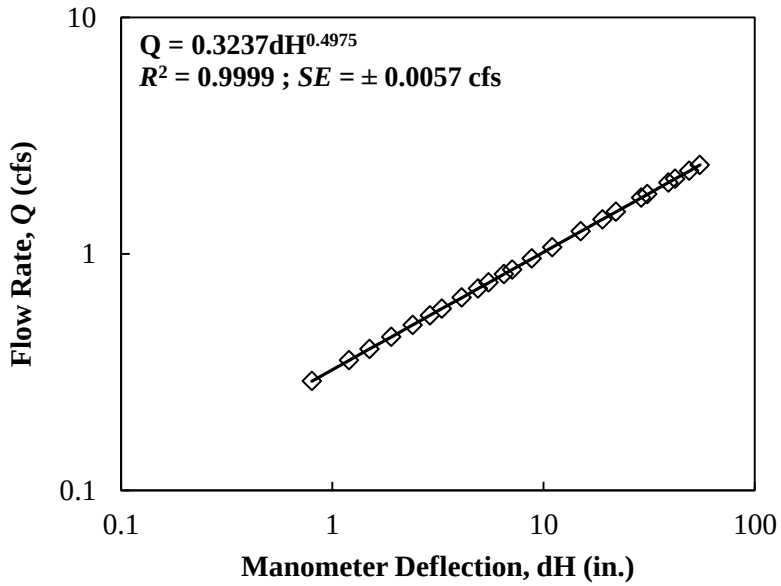

Figure 3.5: Calibration of pump and manometer deflection of bend meter

Source: adapted from Navarro (2004) Figure 3-6

After these two variables are fixed, the flow depth is adjusted to normal depth using the tailgate at the downstream end of the flume. This gate is the control since all of the flows in this study are subcritical flows. The normal depth (y_o) has been measured previously, and the flow resistance determined for several combinations of slope and discharge in uniform flow to achieve a desired shear stress. The tailgate is adjusted until the predetermined value of y_0 is achieved over the full length of the flume. Then the bed shear stress is calculated from the uniform flow equation given by (Sturm 2001):

$$\tau = \gamma_w y_0 S_o \tag{3.7}$$

in which γ_w is the specific weight of water. More details on independent validation of Eq. (3.7) and development of the flow resistance factor with sidewall correction can be found in work by previous investigators in this flume (Ravisanger et al. 2001; Navarro

2004; Hobson 2008). All of the hydrodynamic conditions in this study are shown in Table 3.3.

Table 3.3: Hydrodynamic conditions for flume experiment

Flow Rate Q (m^3/s)	Slope S_o ($\times 10^{-3}$)	Water Depth Y_o (cm)	Average Velocity V (m/s)	Bed Shear Stress τ (Pa)	Froude Number $Fr = \frac{V}{\sqrt{gy}}$	Reynolds Number $\mathrm{Re} = \frac{4RV}{\nu}$
0.0156	2.00	8.66	0.474	1.70	0.514	2.83×10^5
0.0227	1.99	10.95	0.543	2.15	0.523	3.51×10^5
0.0283	3.00	12.65	0.588	2.48	0.528	3.89×10^5
0.0227	3.00	9.60	0.619	2.83	0.638	3.93×10^5
0.0283	3.00	11.00	0.677	3.24	0.651	4.39×10^5

Once the flow rate, water depth, and flume slope had been fixed for the desired shear stress, the flow was stopped using the pump flow valve on the overhead pipe and the flume was allowed to drain into the storage tank. The Shelby tube, which held the settled sample, was inserted into the flume at the hole in the flume bottom and centered over the hydraulic jack. The excess water on top of the sample was suctioned off and then the jack was used to raise the sediment in the tube until it was level with the surrounding bed of the flume. A water content sample was taken using a spatula and the remaining sediment was then covered with a metal plate. The flow was then restarted and the conditions checked before the test began.

To measure the erosion rate during the experiment, a potentiometer was attached to the hydraulic jack head to follow upward movement of the piston electronically. The operator adjusted the jack to keep the sediment level with the surrounding bed as erosion occurred. The voltage output from the cable-pull potentiometer ran through a National

Instruments data acquisition board and then was recorded by a Matlab program. The calibration of the potentiometer is shown in Figure 3.6.

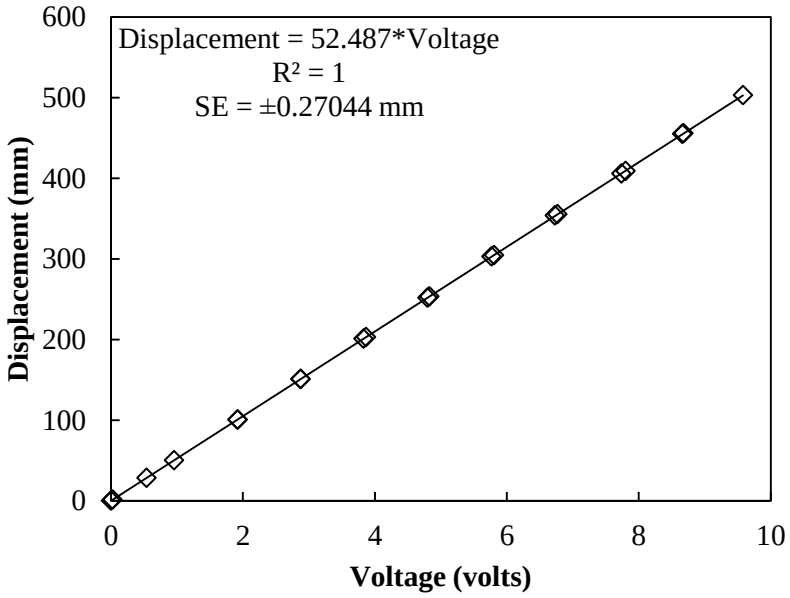

Figure 3.6: Calibration of cable-pull potentiometer

Since the water used in the flume was recirculated after passing the sediment sample, the water began to become cloudy as more of the sediment was eroded. Once the sediment was no longer visible to the opertator, the erosion test ended and the flume was shut down and drained. The water content of the sediment was taken at this point, the depth recorded from the Matlab file, and then the storage tank was refilled for the next erosion trial.

This experimental procedure allowed for a water content measurement to be taken at the beginning and end of each erosion test. These two values were then averaged to produce the water content throught the recorded depth. This procedure also minimized

error by reducing the impact if there was error in one of the measurements. Both the time and depth of the erosion were measured to calculate the erosion rate (E) in $kg/m^2/s$ from:

$$E = 0.001\frac{\Delta D}{\Delta t}\rho_d \tag{3.8}$$

where $\frac{\Delta D}{\Delta t}$ = the slope produced by the Matlab program of the displacement versus time data recorded by the potentiometer. An example of this slope is shown in Figure 3.7 for an experiment using 30% Kaolinite by weight and operating at a bed shear stress of 2.48 Pa.

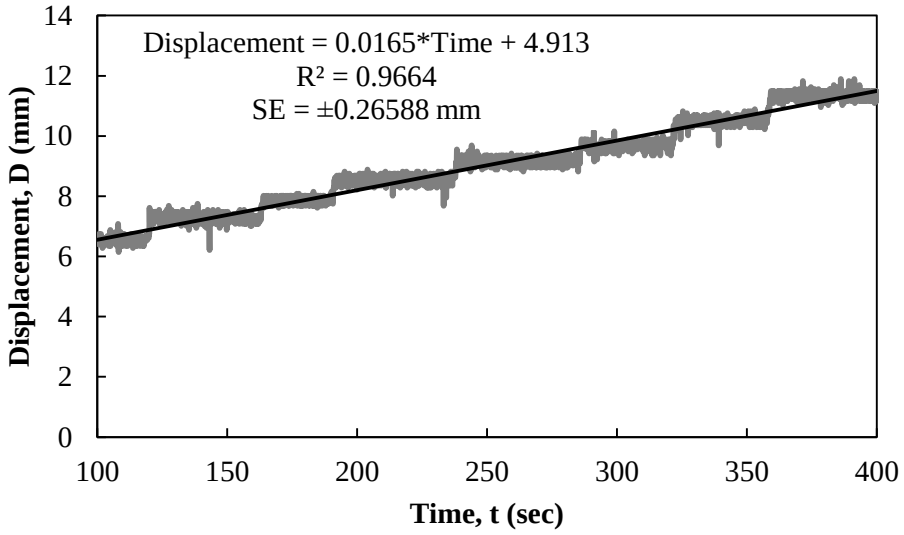

Figure 3.7: Example potentiometer data (time and displacement) for 30% Kaolinite mixture with an applied bed shear stress, τ = 2.48 Pa

The erosion was calculated from the displacement versus time multiplied by the dry density. Once all experiments for a percent kaolinite mixture were completed, the data were then organized by water content and depth in the sample. Groups were formed

from this organization and each group represented an average water content, average depth, and consisted of at least one erosion rate value from each of the five applied bed shear stresses. This method of grouping provided a means to classify the data into groups of similar water content since each applied bed shear stress produced a different eroded depth which precluded reproducing the erosion rate and water content at the same exact depth in a test of a different sample.

Each water content group's erosion rates were then individually plotted against the applied bed shear stress. A Generalized Reduced Gradient (GRG) nonlinear solving method was executed inside of Microsoft Excel's 2010 Solver analysis tool along with Eq. (2.1), $E = M(\tau-\tau_c)^n$, in order to find the best fit line through the erosion data points. The erosion rates and applied bed shear stresses were the input data and the solver iterated on different values of M, τ_c , and n until the best fit line was in agreement with the input data. The solver focused on minimizing the summed square of the residuals, or *SSE*, and terminated when the last five iterations of SSE had a relative change less than 1%.

$$SSE = \sum \left(y_i - \hat{y}_i \right)^2 \tag{3.9}$$

The experimental constants M and n are different for each data group and sediment mixture. The critical shear stress, τ_c, is defined as the shear stress at which there is a zero erosion rate for a particular sediment mixture and water content. Thus, τ_c equates to the x-intercept of the best fit line, n is the degree of curvature of the best fit line, and M is the erosion rate scale factor of this line. Previous studies in this flume have followed the same erosion testing procedure and have shown the credibility and accuracy of these procedures (e.g. Ravisangar 2001; Ravisangar et al. 2001, 2005; Navarro 2005; Hobson 2008; Wang 2013).

3.4 Summary of Experimental Procedures

This chapter describes the experimental procedures used to measure the sediment erodibility properties of the sand-kaolinite mixtures. All sediment property tests and erosion tests are explained in detail to describe the level of preparation used to obtain each measurement. The next chapter will cover the values obtained using these experimental methods which are used to correlate the critical shear stress with the physical properties of the sediment. These experiments complement the work of Navarro (2004), Hobson (2008), and Wang (2013) by analyzing sediments with particle sizes covering the transition between fine and coarse particle sizes. Navarro and Hobson used these same procedures on mostly coarse natural Georgia sediments and Wang followed these same guidelines to experiment on fine silt-kaolinite sediments mixed in the laboratory. The measured critical shear stresses of the sand-kaolinite sediments in this study will bridge the gap between the data and equations of the previous researchers. The relationship among these three data sets will be explained in the next two chapters.

CHAPTER IV

EXPERIMENT RESULTS

4.1 Sediment Properties

Covered in this chapter are the results from the size distribution measurements, Atterberg limits, water content and density measurements, and the slurry measurements taken right after mixing a specimen. Size distribution measurements were performed on samples prepared in the same manner called for in preparation of an erosion test. Size distributions were completed for mixtures with 100%, 80%, 70%, 50% and 30% kaolin percentages by weight. Water content measurements were performed during erosion tests by taking the wet weight and dry weights of samples at specific depths of a mixed specimen during an erosion test. Water content measurements were taken before and after each erosion trial which allowed for water contents to be taken at multiple depths of one mixture. Erosion tests were run at five different shear stresses as shown in Table 3.3 and each shear stress erosion test was repeated at least three times. This called for at least 15 experiments to be performed for each kaolinite-sand mixture, at the five shear stresses, and three times for each shear stress to reduce error through replication. The 100% Kaolinite case was the only exception, since only five experiments were run with this mixture; one for each bed shear stress. This mixture was analyzed mainly to check that the experimental procedures listed above produced results similar to past experiments that tested a similar kaolinite. The temperature, pH, and conductivity of each specimen were taken just after mixing with an electronic blender, and were taken during the setup of each of these 15 experiments.

4.1.1 Size Distribution and Atterberg Limits

Size distributions of the mixtures of fine sand and kaolinite were tested along with the pure fine sand and 100% kaolinite. A size distribution for each mixture was

performed on the top third, middle third, and bottom third of the sample. This was done by following the same procedure called for in preparation of an erosion experiment, including allowing the sample to settle for 24 hours. The mixed samples were checked to determine if consistent settling occurred throughout the sample with a constant distribution of both sand and kaolinite in the whole mixture. As shown in Figure 4.1, each mixture was evenly distributed throughout the height of the sample. This means that even though the density of the specimen changes throughout the height of the sample, the proportion of sand and kaolinite is consistent from top to bottom and the only stratification is from density and water content variations.

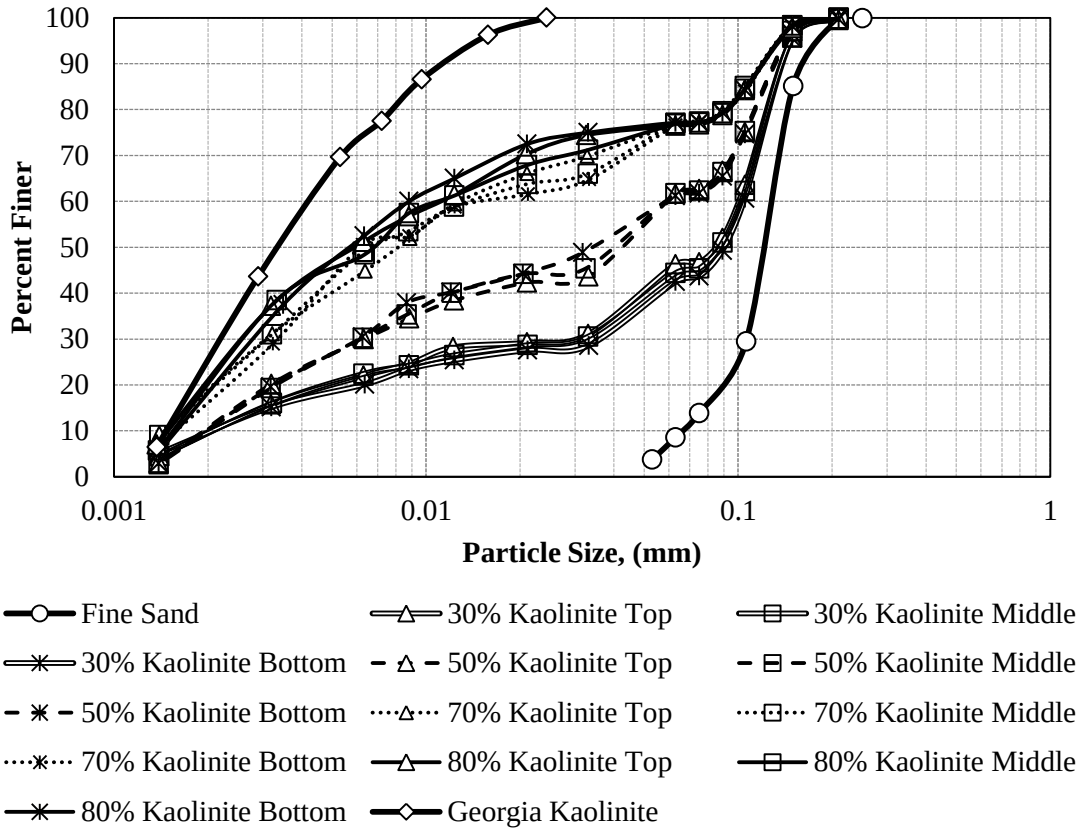

Figure 4.1: Grain size distributions for all mixtures of sand and kaolinite.

Measures of the size distribution can be taken from Figure 4.1. These values (d_{xx}) are d_{60}, d_{50}, d_{30}, and d_{10} and they represent, respectively, the particle size that 60%, 50%, 30%, and 10% of that mixture's particles by weight are smaller than. There are two key observations from Figure 4.1. First, the size distribution parameters for each mixture are consistent from top to bottom layers, showing that in each mixture there is a consistent spread or distribution of particle sizes throughout the height of the sample. Second, as the kaolinite content increases the values of d_{xx} proportionally decrease.

Two important parameters can be calculated from the d_{xx} values to demonstrate the grading of a sediment. The coefficient of curvature (C_c) and the coefficient of uniformity (C_u) are defined as:

$$C_u = \frac{d_{60}}{d_{10}} \tag{4.1}$$

$$C_c = \frac{d_{30}^2}{d_{10} d_{60}} \tag{4.2}$$

Values of C_u and C_c are typically applied to coarse sediments which are classified as sediments in which at least 50% of the sediment is retained on the #200 sieve (0.075mm) or higher. As can be noted in Table 4.1, this applies directly to both the fine sand and the 30% Kaolinite mixture.

Shown along with the size distribution parameters in Table 4.1 is the Clay Size Fraction (*CSF %*) which represents the percent of the sediment which is finer than 0.002 mm by weight. These values were taken from the above figure and increase as the kaolinite percentage increases.

Table 4.1: Values from the size distribution chart used to classify mixtures

Kaolinite Content and Location	d_{60} (mm)	d_{50} (mm)	d_{30} (mm)	d_{10} (mm)	C_c	C_u	CSF (%)	% Fines
0% (Fine Sand)	0.130	0.122	0.106	0.079	1.1	1.6	0.0	8%
30% Top	0.101	0.086	0.031	0.002	4.5	48.1	9.5	47%
30% Middle	0.102	0.088	0.032	0.002	4.8	48.6	9.5	45%
30% Bottom	0.104	0.09	0.036	0.002	5.9	49.5	9.6	43%
50% Top	0.060	0.043	0.006	0.002	0.3	31.6	10.5	61%
50% Middle	0.059	0.041	0.006	0.002	0.3	29.5	10.5	61%
50% Bottom	0.059	0.034	0.006	0.002	0.3	29.5	10.5	61%
70% Top	0.013	0.008	0.003	0.0015	0.5	8.7	19.1	76%
70% Middle	0.014	0.007	0.003	0.0015	0.4	9.3	19.0	76%
70% Bottom	0.015	0.006	0.003	0.0016	0.4	9.4	16.0	76%
80% Top	0.012	0.006	0.003	0.0016	0.4	7.5	21.0	77%
80% Middle	0.012	0.007	0.003	0.0016	0.4	7.5	20.5	77%
80% Bottom	0.012	0.006	0.003	0.0016	0.4	7.5	18.0	77%
100% (Kaolinite)	0.004	0.003	0.002	0.0005	2.2	8.2	25.0	100%

The Atterberg values of liquid limit, plastic limit, and plasticity index were measured for each sediment mixture and are shown in Table 4.2. The 30% Kaolinite mixture is defined as nonplastic according to the ASTM standard when the operator is unable to form a groove during the Casagrande cup test due to granular responses or is unable to obtain a water content that allows the required number of blows (see ASTM D4318-10 (2010b) for more details about nonplastic classification). The kaolinite contents and Atterberg values are positively related, i.e., as the kaolinite content increases so too do the Atterberg values. This is also displayed in Figure 4.2 which is a graphical representation of the measured Atterberg values.

Table 4.2: Atterberg values for all mixtures

Kaolinite Content by Percent Weight	30% Kaolinite	50% Kaolinite	70% Kaolinite	80% Kaolinite	100% Kaolinite
Liquid Limit	N/A	23%	29%	35%	45%
Plastic Limit	N/A	19%	23%	26%	29%
Plasticity Index	NonPlastic	4%	6%	9%	16%

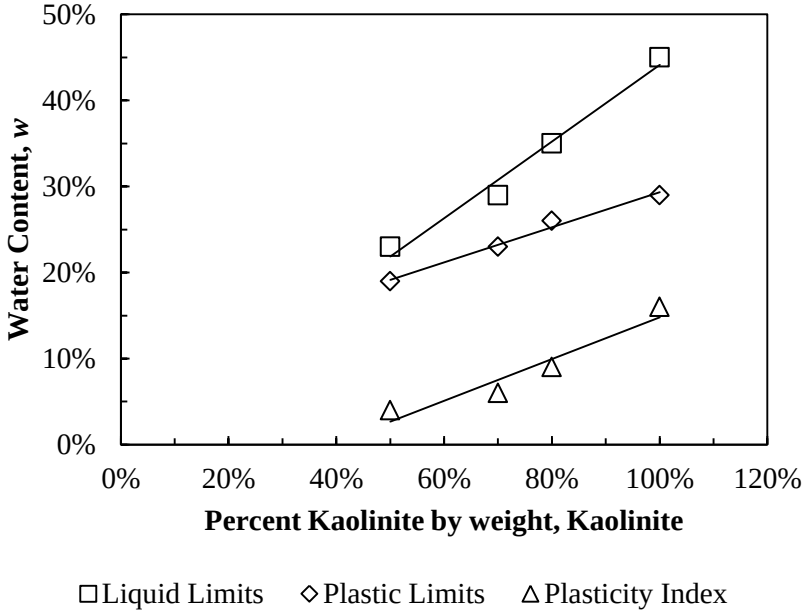

Figure 4.2: Atterberg values for each plastic mixture

The linearity of the liquid limit, plastic limit, and the plasticity index were analyzed using the decimal fraction of kaolinite content, *Kaolinite*, as the dependent variable and the water contents in decimal fractions for each respective Atterberg value.

$$w_{LL} = 0.4462 \times Kaolin - 0.0046 \qquad R^2 = 0.98 \; ; \; SE = \pm 0.0162 w_{LL} \qquad (4.3)$$

$$w_{PL} = 0.2038 \times Kaolin + 0.0896 \qquad R^2 = 0.99 \; ; \; SE = \pm 0.0060 w_{PL} \qquad (4.4)$$

$$I_P = 0.2423 \times Kaolin - 0.0942 \qquad R^2 = 0.92; \; SE = \pm 0.0179 I_P \qquad (4.5)$$

As shown in these equations and Figure 4.2, the liquid limit is more dependent on the kaolinite content whereas the plastic limit and plasticity index are affected almost equally. All Atterberg values increase with an increase in kaolinite content by weight. The recorded plasticity index is low for kaolinite sediments. Typical plasticity index values for kaolinite range from 21-26% (Ranjan and Rao 2000).

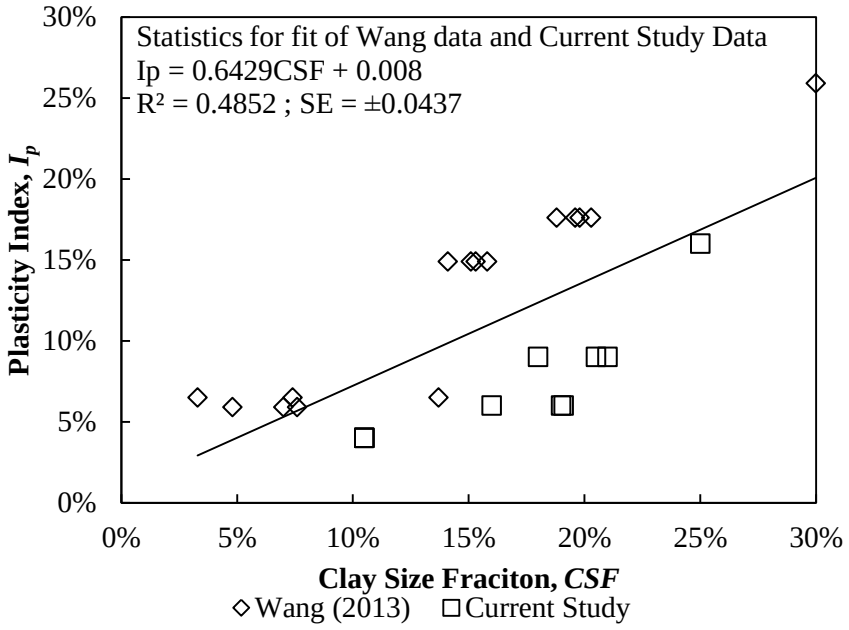

Figure 4.3: Plasticity index and clay size fraction

Figure 4.3 contains the plasticity index values from each mixture of kaolinite in comparison to the clay size fraction, *CSF,* for each mixture in the current study and those of Wang (2013). Table 4.1 has the *CSF* for each layer of each kaolinite mixture and these were plotted with the corresponding plasticity index for that mixture.. The plasticity index, $I_{p,}$ has been studied in past research with regards to its effect on the erosion threshold, and cohesive erosion behavior has been found to occur in sediments with I_p >

7% (e.g., Lambe and Whitman, 1979; Winterwerp and van Kesteren 2004, Whitlow, 2001). For a plasticity index value of 7%, the best fit line in Figure 4.3 gives a *CSF* of 10%. This means that for all mixtures with a *CSF* > 10%, cohesive erosion behavior is expected. The 50% kaolinite mixture has a *CSF* of 10.5% and the 70%, 80%, and 100% kaolinite mixtures all have values above 10%.

The activity of a sediment is a property derived from the plasticity index that is used to define the erodibility of a sediment with respect to the clay size fraction. The activity of a sediment relates the plasticity index to the clay size fraction and thus displays the degree of effect that the clay has on the plasticity index.

$$A = \frac{I_P}{CSF} \tag{4.6}$$

From Figure 4.3 the activity is taken as the slope of the best fit line through the points of both data sets. The activity is found to be 0.6429, which falls in the range of previously found activities for kaolinite, from 0.38 to 0.67 (Lambe and Whitman 1979, Jacobs 2011).

4.1.2 Water Content and Bulk Density

Water content measurements were taken before and after each erosion trial and averaged to produce the water content throughout that depth layer. For one Shelby tube, containing one specific mixture of kaolinite and fine sand, there were anywhere between three and seven erosion trials performed at the same shear stress. This was due to the different depths eroded amongst various bed shear stresses and the number of tests the sample total depth could accommodate. Since different shear stresses caused different levels of erosion, it was not possible to take erosion measurements at the same depth for all Shelby tubes. Therefore the water contents were compared with depth for all mixtures to check that consistent variation of water content was occurring throughout the height of the Shelby tube. These comparisons can be found in Figure 4.4 (a) through (e).

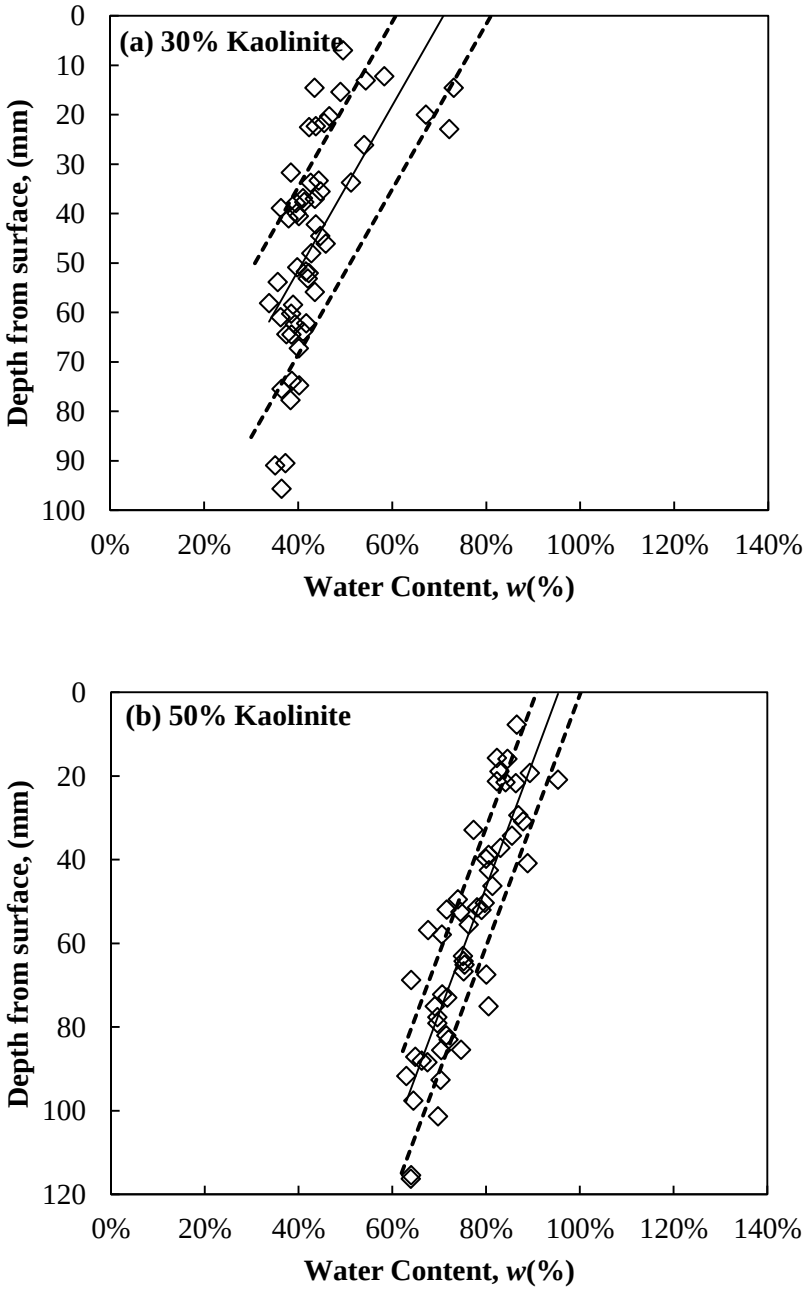

Figure 4.4: Water contents at assorted depths with ±1 standard deviation for mixtures of (a) 30% Kaolinite, (b) 50% Kaolinite. (c) 70% Kaolinite, (d) 80% Kaolinite, and (e) 100% Kaolinite

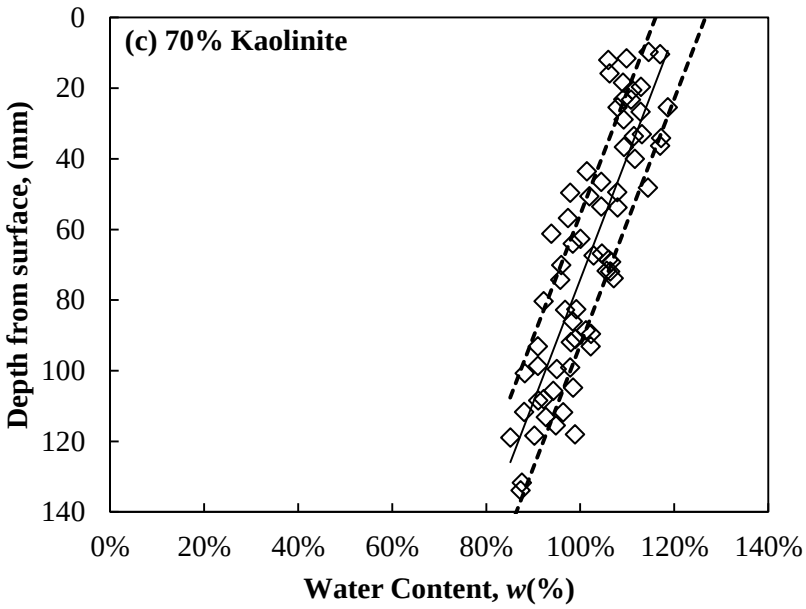

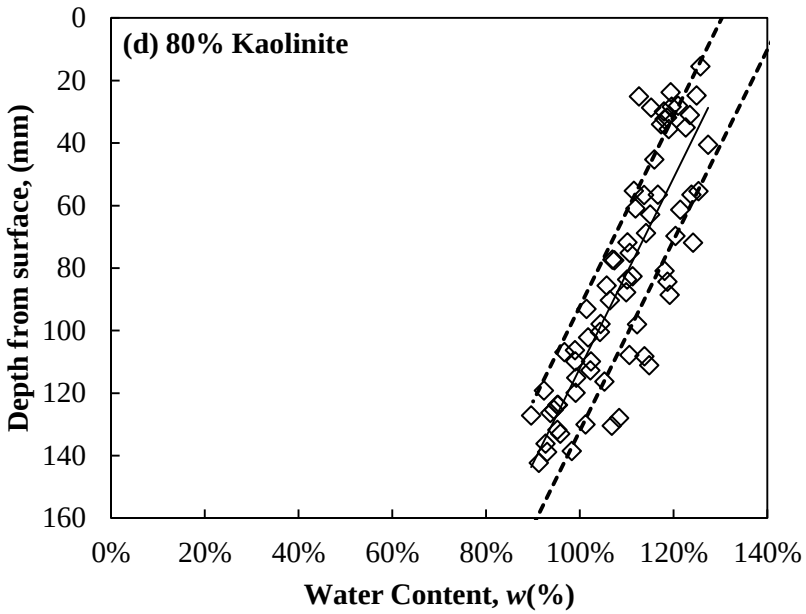

(Figure 4.4 Continued)

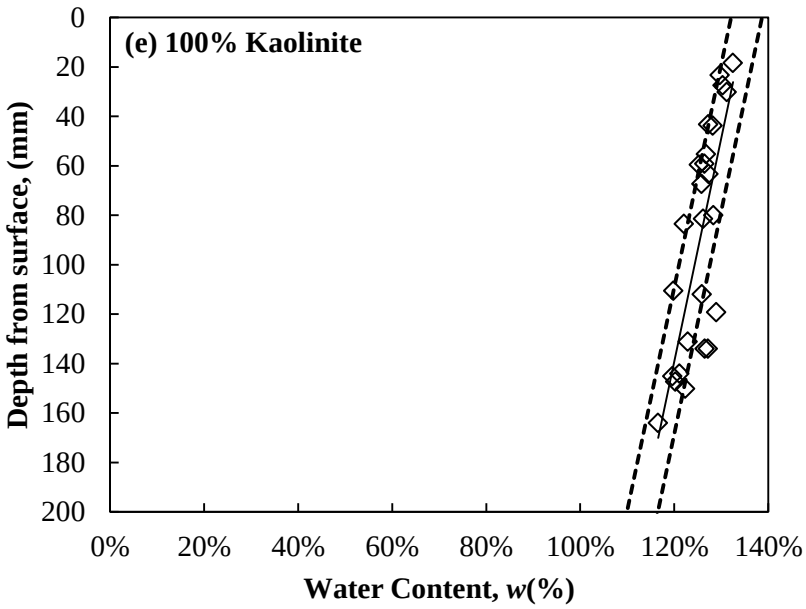

(Figure 4.4 Continued)

Shown in Table 4.3 are the statistical data associated with the water content versus depth lines for each mixture. Figure 4.5 shows the slopes of water content versus depth for all Kaolinite percent mixtures. The standard error of estimate (*SE*) for each mixture's best fit line is shown as a dotted line to display the confidence interval of the data. In the equation, *N* is the number of data points.

$$SE = \sqrt{\frac{SSE}{N-2}} \tag{4.7}$$

Table 4.3: Statistical data of best fit lines for all water content vs. depth lines

% Kaolinite	Slope of best fit line (*w*%/mm)	*SE* of water content (%)	R^2 of Best Fit Line	Range of Water Content (*w*%)
30%	-0.0025	6.5%	0.41	34-73%
50%	-0.0025	4.1%	0.74	63-95%
70%	-0.0021	4.5%	0.72	85-119%
80%	-0.0024	5.5%	0.72	90-127%
100%	-0.0007	2.6%	0.61	117-132%

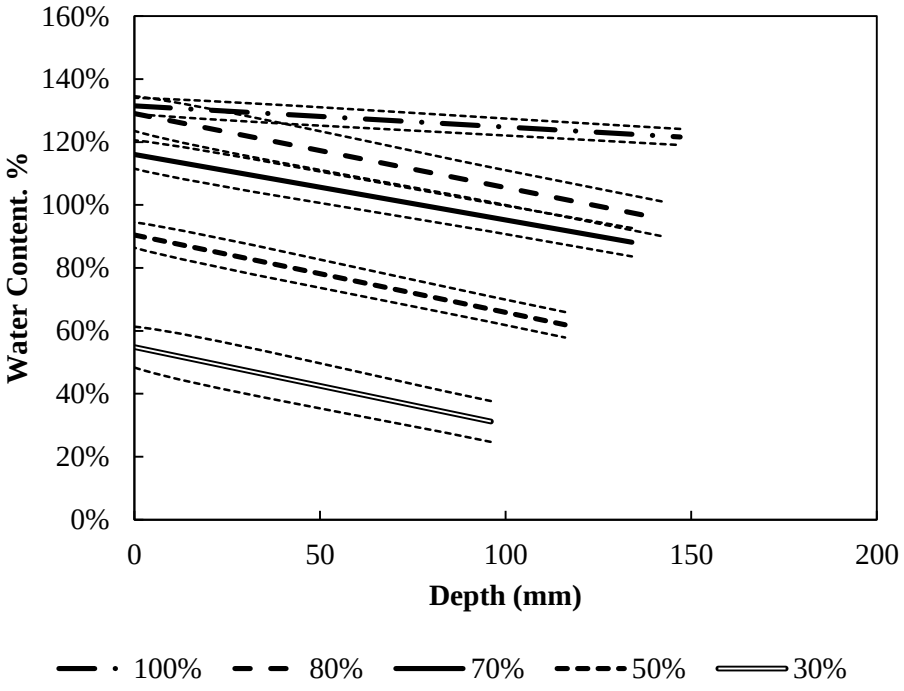

Figure 4.5: Water content vs. depth for all mixtures with boundaries of ±1 *SE* as dotted lines

From Table 4.3 and Figure 4.5, it can be observed that the slopes for mixtures with 80%, 70%, 50%, and 30% Kaolinite are similar. However, the values in the range of water content increase as Kaolinite content increases. This is due to the increase in clayey particles which have a higher surface area to volume ratio. Even though all mixtures were prepared in the same manner, there are slight variations in the water contents at the same depths. This variation is illustrated in Figure 4.5 through the standard estimate of error for that mixture. For all mixtures, this error was between 2.5% and 6.5%. Although mixtures were prepared following identical procedures, there are forms of operational and experimental error in taking the sample and measuring the wet and dry masses to determine water content that would account for the observed error. The spread of the data can also be observed by looking at the R^2 value for each best fit line. This value shows the linearity of the water content versus depth. Most of the mixtures are fairly linear, with the 30% kaolinite mixture having the least linearity. The clay in kaolinite retains larger water contents than sand grains and more consistently so.

Bulk density is calculated from water content using Eq. (3.6). Bulk density is expected to increase as depth from the sediment surface increases. Figure 4.6 shows the bulk densities of different mixtures located at various depths. These data points came from each averaged water content value which was calculated from each measurement before and after erosion tests. These values were then used to calculate a bulk density for that specific depth.

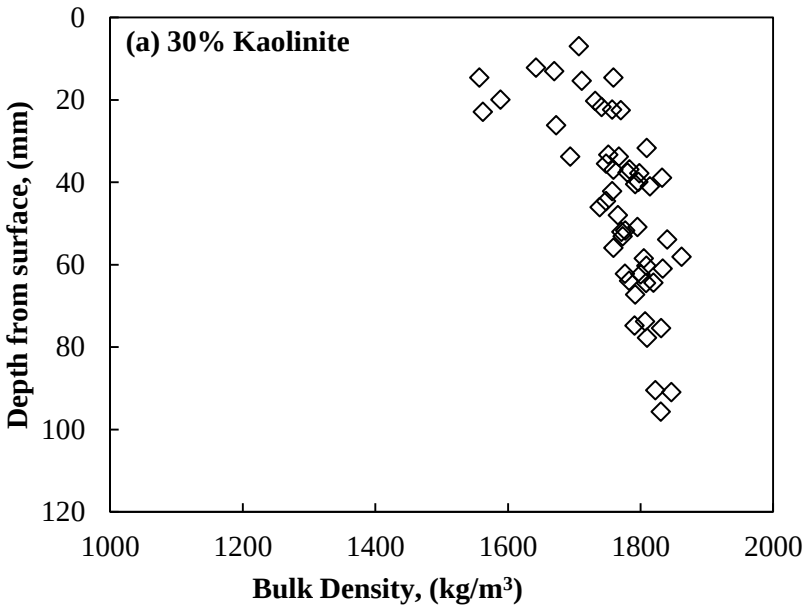

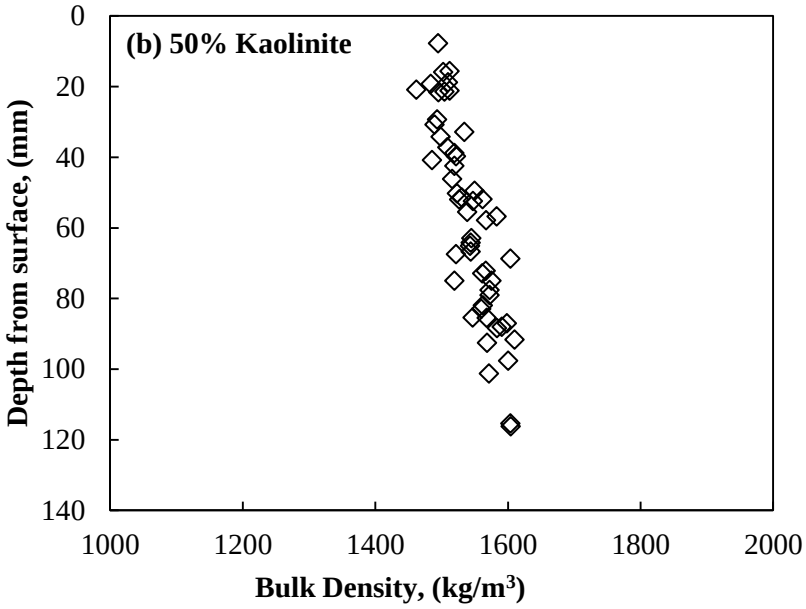

Figure 4.6: Bulk densities at assorted depths for each shear stress for (a) 10% Kaolinite, (b) 50% Kaolinite, (c) 70% Kaolinite, (d) 80% Kaolinite, and (e) 100% Kaolinite

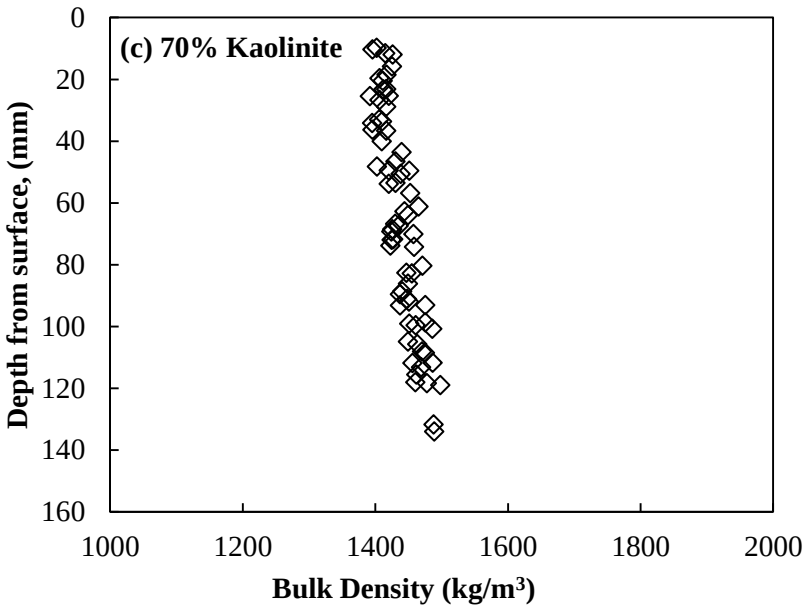

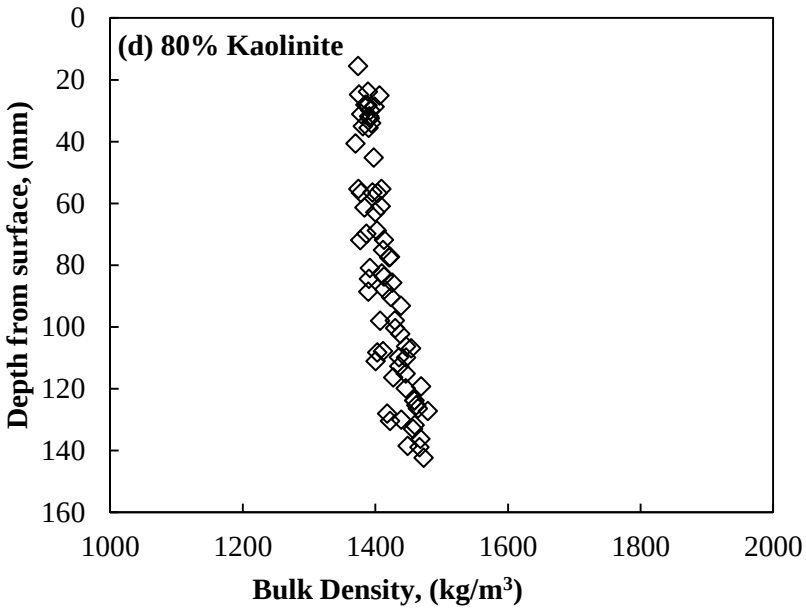

(Figure 4.6 Continued)

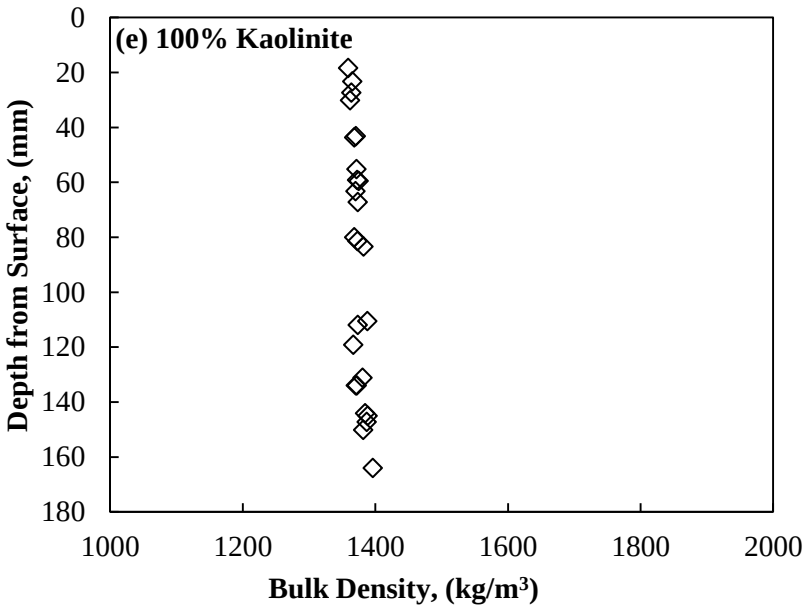

(Figure 4.6 Continued)

The bulk densities of each mixture increase as depth increases. As kaolinite content increases, the density increase for the same change in depth is not as steep. This is displayed in the figures above or also in Table 4.4 which shows the inverse slope or $\frac{\Delta\rho}{\Delta D}$, standard error of estimate, and R^2 value of the best fit line along with the range of bulk densities that each mixture contains. The slope of each best fit line decreases as the kaolinite content increases which shows that there is less variation in bulk density with depth for higher kaolinite contents. The range of bulk densities also decreases as kaolinite content increases which shows that there is less stratification of density throughout depth for higher kaolinite contents.

Table 4.4: Bulk density variation with depth for each mixture

Kaolinite content by weight (%)	Slope of best fit equation (kg/m^3/mm)	*SE* of bulk density (kg/m3)	R^2 of best fit line	Range of Bulk Density (kg/m^3)
30%	2.09 ± 0.31	48.73	0.47	1557 - 1862
50%	1.16 ± 0.10	18.91	0.75	1462 - 1610
70%	0.66 ± 0.05	13.92	0.74	1392 - 1498
80%	0.67 ± 0.05	16.02	0.71	1370 - 1480
100%	0.15 ± 0.03	5.94	0.60	1359 - 1396

4.1.3 Temperature, pH, and Conductivity

The temperature, pH, and conductivity of each mixture were recorded immediately after dispersion and before the specimen was poured into the Shelby tube and allowed to settle. The conductivity and pH probes of the Oakton Waterproof PC 300 were dipped into the specimen to a consistent depth. The conductivity probe has a temperature sensor built into it which recorded information as well and compensates for temperature variation in conductivity and pH. These three values were taken for each mixture and the collective data are shown in Table 4.5 along with average, standard deviation, and relative standard deviation values.

Table 4.5: Temperature, pH, and conductivity for all mixtures

Mixture	Temperature (^{o}C)		pH		Conductivity (µS)	
	Avg ± St. dev.	Relative St. Dev.	Avg ± St. dev.	Relative St. Dev.	Avg ± St. dev.	Relative St. Dev.
Tap Water	21.7 ± 0.2	0.84%	6.64 ± 0.09	1.41%	125 ± 13	10.65%
30% Kaolinite	22.9 ± 0.7	2.96%	5.00 ± 0.04	0.90%	426 ± 36	8.39%
50% Kaolinite	22.7 ± 0.7	3.03%	4.86 ± 0.07	1.51%	529 ± 45	8.43%
70% Kaolinite	23.0 ± 0.9	4.07%	4.71 ± 0.04	0.95%	647 ± 37	5.74%
80% Kaolinite	23.8 ± 0.5	2.23%	4.67 ± 0.03	0.62%	680 ± 35	5.12%
100 % Kaolinite	22.1 ± 0.2	0.74%	4.58 ± 0.03	0.64%	795 ± 23	2.93%

As shown in Table 4.5, the temperature of these mixtures was within the range of 22-24 ^{o}C and fairly consistent for each mixture, but the pH and conductivity changed with the proportion of kaolinite. As the percentage of kaolinite increased, the pH decreased and the conductivity increased. This is shown graphically in Figure 4.7 along with the confidence limits of plus or minus one standard deviation of the data. Tap water is shown as the 0% Kaolinite.

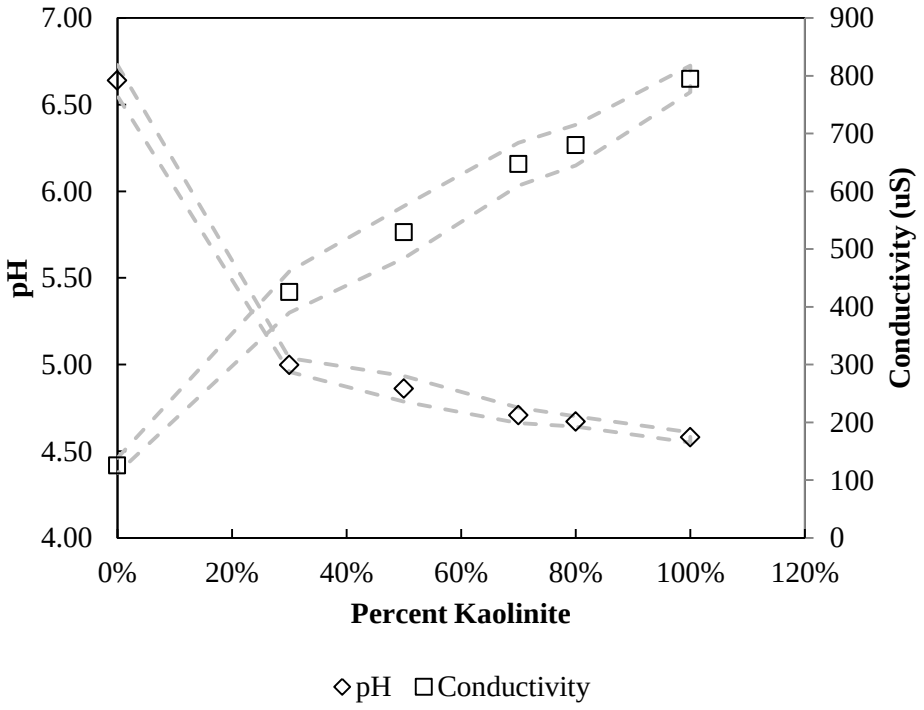

Figure 4.7: Conductivity and pH values for all mixtures with boundaries of ±1 standard deviation

In order to accurately assess this data, the relative standard deviation is also calculated to show the ratio of the standard deviation to the mean. This value is very

small for pH, meaning that the pH values are consistent between different measurements. The relative standard deviation is higher for conductivity values, and this could be from instrument uncertainty or the variation in depth of the probe in the mixture was an important factor in conductivity but not for pH.

4.2 Erosion Data

Erosion rates of each sediment were calculated by multiplying the measured eroded sediment displacement over time ($\frac{\Delta D}{\Delta t}$) and the dry density ($\rho_d$). Since water content increases as depth increases, and the erosion rate depends on the water content, different erosion rates are found for different depths. This relationship is shown in Figure 4.8. As water content decreases the erosion rate is smaller. This can be seen in the figure when comparing different groups. Group 1 is the top group, located at the surface and characterized by the highest water content, and each subsequent group represents a decrease in water content and thus a lower depth. Each group was chosen by separating all of the erosion data for a specific Kaolinite % and sorting by water content and depth, then separating the data into groups that have similar values of erosion rate. The GRG nonlinear solver was then applied to each group individually as described in Chapter 3.

As shown in Figure 4.8, when looking at one individual group, as the applied bed shear stress increases, so does the erosion rate. This is expected since more erosion forces are acting on the sediments, more sediments should be eroded. This increase in erosion with respect to an increase in bed shear stress is more dramatic for the groups closest to the top of the sample, Groups 1 and 2.

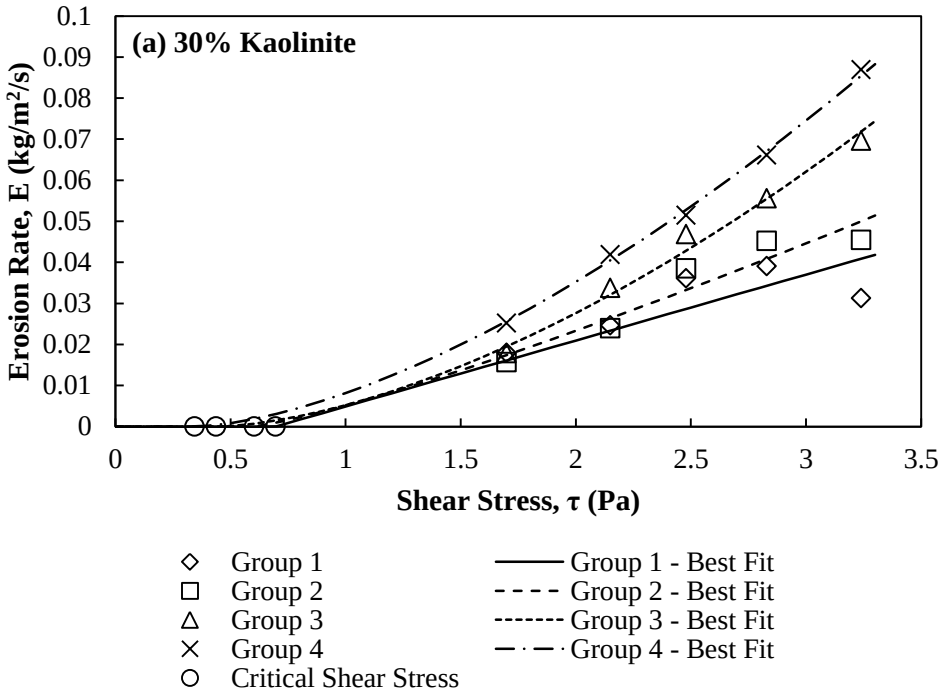

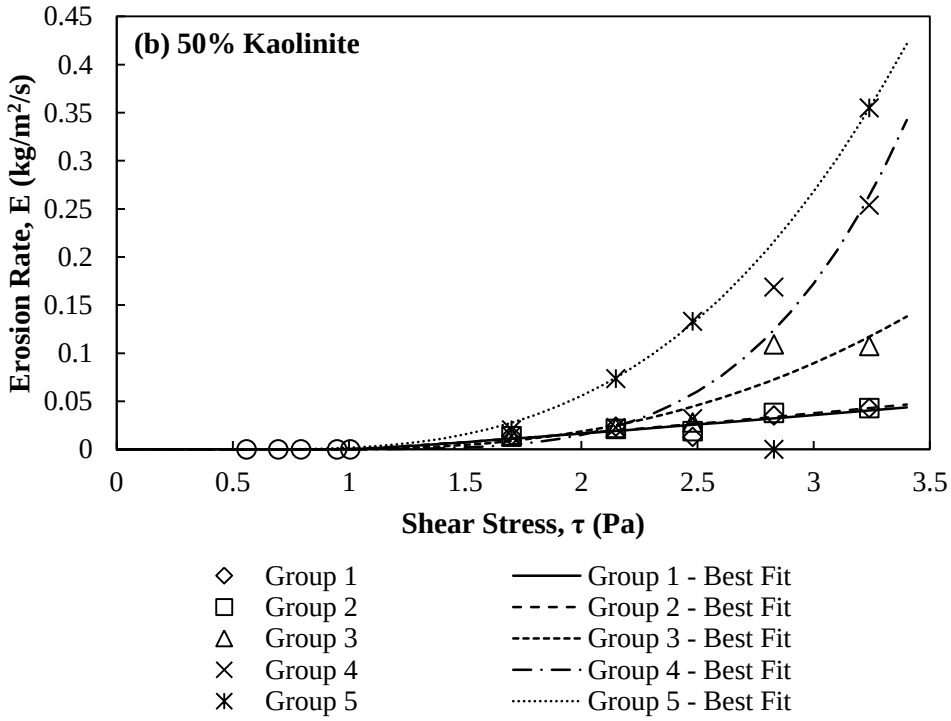

Figure 4.8: Erosion rate versus bed shear stress with best fit lines for each group of (a) 30% Kaolinite, (b) 50% Kaolinite, (c) 70% Kaolinite, (d) 80% Kaolinite, and (e) 100% Kaolinite

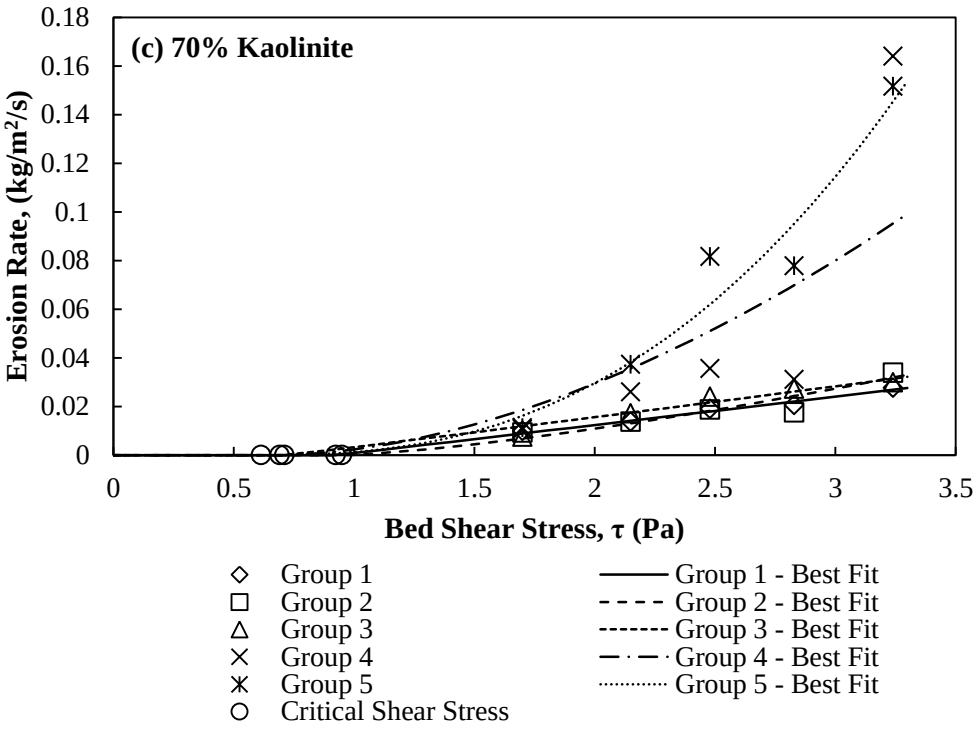

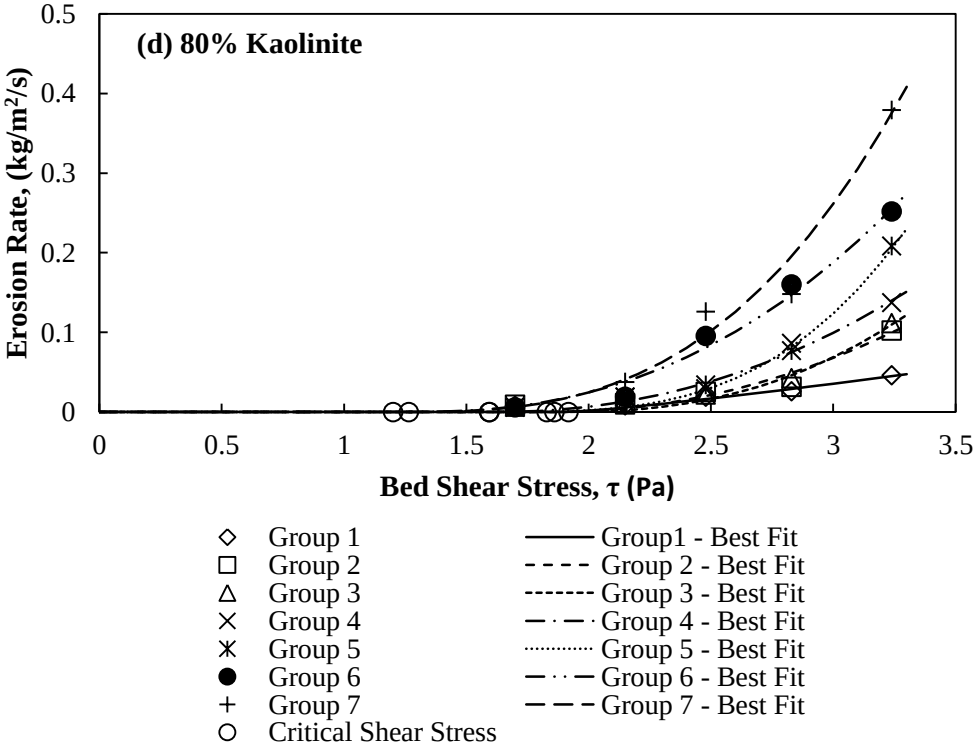

(Figure 4.8 Continued)

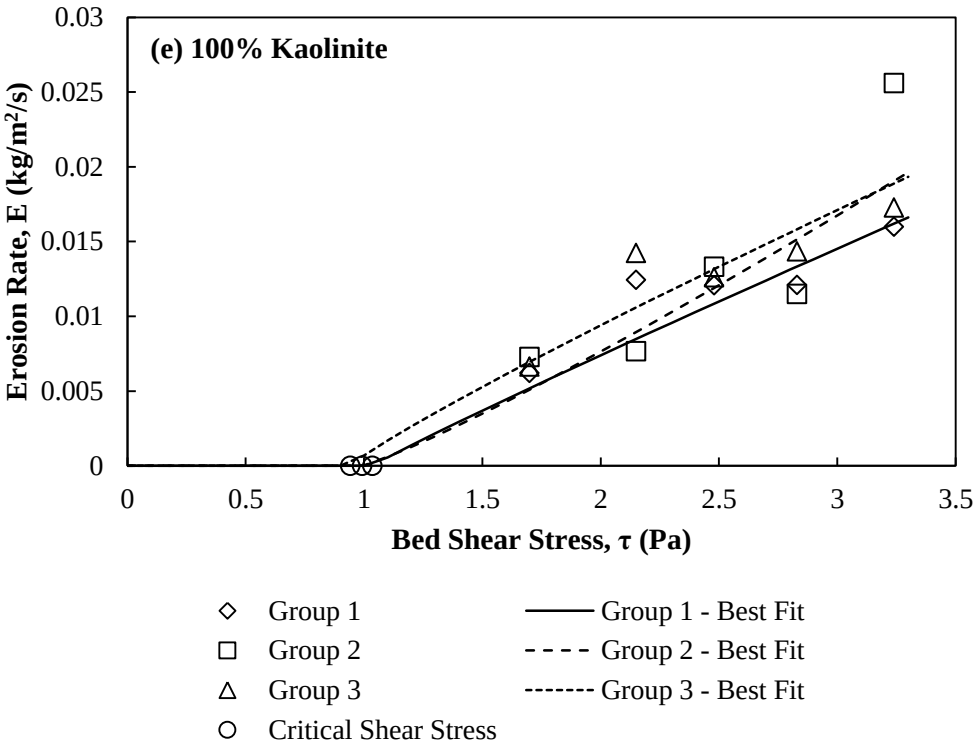

(Figure 4.8 Continued)

The experimental values of *M*, *n*, and τ_c for each group and for each percent Kaolinite mixture were determined using a nonlinear solver and graphically represented in Figure 4.8. These values are compiled in Table 4.6 as well. As water content increases, *n* generally increases for groups of the same percent kaolinite. The critical shear stress is found to decrease as water content increases. The critical shear stress is also found to increase as the percent kaolinite or *CSF* increases. Fine sand has a higher bulk density than consolidated clay, but has a lower erosion threshold (Grabowski 2011). This study shows that as sand content increases the erosion threshold decreases, which is consistent with other studies that show a negative correlation between sand content and critical shear stress (Gerbersdorf et al. 2005, 2007).

Table 4.6: Experimental values for best fit curves of erosion data

Kaolinite Percent	Group #	Water Content (*w*%)	*CSF*	Average Depth (mm)	Critical Shear Stress (Pa)	*M* Value	*n* Value
30%	1	38%	9.5%	63.4	0.70	1.61×10^{-2}	1.00
	2	42%	9.5%	50.6	0.60	1.56×10^{-2}	1.20
	3	44%	9.5%	35.3	0.44	1.33×10^{-2}	1.64
	4	54%	9.5%	18.6	0.34	1.59×10^{-2}	1.58
50%	1	64%	10.5%	98.0	1.01	1.65×10^{-2}	1.12
	2	69%	10.5%	80.2	0.95	1.56×10^{-2}	1.22
	3	74%	10.5%	68.7	0.79	1.14×10^{-2}	2.61
	4	80%	10.5%	47.8	0.70	4.81×10^{-3}	4.29
	5	86%	10.5%	25.5	0.56	1.88×10^{-2}	2.98
70%	1	91%	19.0%	106.9	0.92	1.15×10^{-2}	1.01
	2	98%	18.0%	82.0	0.95	1.01×10^{-2}	1.38
	3	102%	17.0%	71.4	0.71	1.20×10^{-2}	1.04
	4	106%	16.0%	51.3	0.69	1.83×10^{-2}	1.76
	5	113%	16.0%	26.9	0.61	1.31×10^{-2}	2.49
80%	1	95%	21.0%	127.2	1.92	3.24×10^{-2}	1.18
	2	101%	21.0%	111.7	1.83	4.92×10^{-2}	2.06
	3	106%	20.5%	103.6	1.86	4.98×10^{-2}	2.45
	4	109%	20.5%	90.6	1.60	4.78×10^{-2}	2.16
	5	112%	20.0%	70.3	1.59	4.15×10^{-2}	3.21
	6	116%	19.0%	57.6	1.27	5.10×10^{-2}	2.37
	7	122%	18.0%	45.4	1.20	4.76×10^{-2}	2.90
100%	1	121%	25.0%	134.5	1.04	7.64×10^{-3}	0.95
	2	126%	25.0%	85.1	0.99	7.58×10^{-3}	1.14
	3	131%	25.0%	48.2	0.94	8.93×10^{-3}	0.90

Values of critical shear stress range from 0.34 Pa to 1.92 Pa (Table 4.6). For each sediment, τ_c increases with depth. This increase with depth is less steep for the 100% Kaolinite mixture. Critical shear stress is fairly constant throughout the depth for the 100% kaolinite mixture but for the mixtures of both sand and kaolinite the τ_c varies much more as the depth increases. Since sand has a higher density than kaolinite, for mixtures with larger percentages of sand, the total depth of the settled specimen was much smaller than the total depth of pure kaolinite samples. The mixtures were based on percent by weight, which produced varying heights of samples in the Shelby tubes due to varying total mixture densities between sand and kaolinite.

4.3 Validation of Flume Erosion Technique

To check that this method of testing erosion rates produces accurate erosion results, a coarse sand was used to prove that the critical shear stress obtained from the experiment matched that of the Shields parameter which is a function of the median particle size (Shields 1936). Shields' parameter, τ_{*_c}, is the ratio of applied bed shear stress to the gravitation force per unit volume at critical conditions.

The experiment procedure described in Chapter 3 was used to measure the erosion of the coarse sand at the five applied bed shear stresses described in Table 3.3 and the calculation method described in the previous section was utilized to determine the critical shear stress. This measured critical shear stress was then applied to calculate the measured Shields parameter. This measured Shields value was compared with the predicted Shields parameter to judge if the erosion test produced accurate values of critical shear stress. Figure 4.9 displays the erosion rates and best fit line that determined the experimental values of *M*, *n*, and τ_c for the coarse sand. These values are also shown in Table 4.7 with a comparison of the predicted values and the measured values. The measured value falls in the range of accepted predicted Shields values which means that

the flume procedure and equipment produce erosion rates within an acceptable range. This validates the use of this flume and procedure to estimate the erosion of sediments.

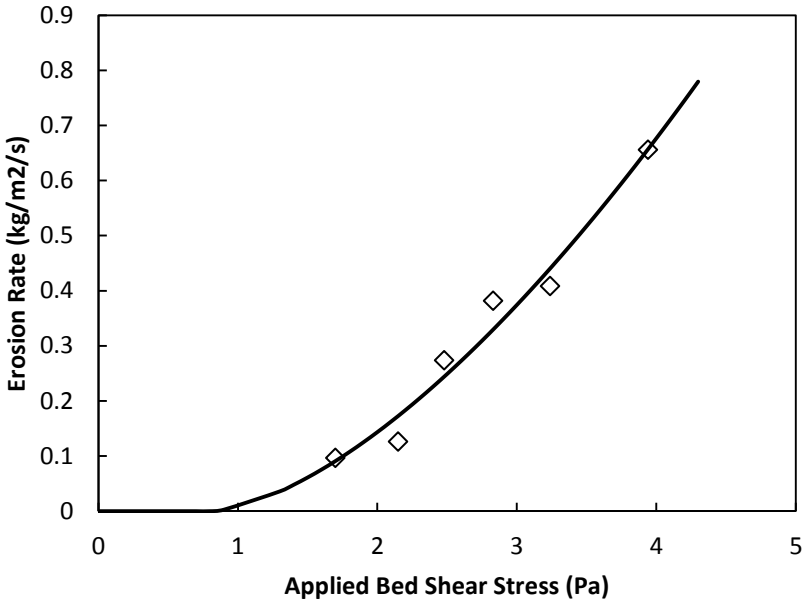

Figure 4.9: Estimation of the erosion experimental values for coarse sand

Table 4.7: Comparison of predicted and measured Shields parameter

	Variable	Value
Predicted Values	d_*	27.8
	τ_{*c} Predicted	0.035-0.046
Experimental Values	τ_{*c} Measured	0.045
	τ_c (Pa)	0.806
	M	0.108
	n	1.574

4.4 Summary of Experimental Results

The previous chapter described the methods used to obtain the sediment and erosion properties of each sediment mixture. This chapter described in depth the findings of those procedures and how the variation of kaolinite in the sediment mixture affected each property. It has been shown that as kaolinite increases bulk density decreases, critical shear stress increases, water content increases, conductivity increases, pH decreases, and d_{50} decreases. All of these relationships with kaolinite content are connected but increase or decrease in dissimilar proportions. The primary association made is that as kaolinite content increases so does critical shear stress, excluding the 100% kaolinite mixture. This connection will be discussed in the next chapter along with how these findings relate to past research.

CHAPTER V

ANALYSIS AND DISCUSSION

Prior studies developed regression equations from laboratory flume erosion tests to predict critical shear stress of field sediments in Georgia, which were mostly coarse-grained (d > 0.062 mm) but with d_{50} < 1.0 mm (Navarro 2004 and Hobson 2008), or laboratory mixtures of kaolinite and silt which could be classified as fine-grained sediments (d < 0.062 mm) (Wang 2013). However, both the coarse and fine sediments contained some distribution of clay size fraction (defined as the fraction finer than 0.002 mm by weight). The percent by weight of kaolinite (or more specifically the clay size fraction) influences several physical properties that determine sediment erodibility. Specifically: (1) the higher surface area to volume ratio of clay particles cause the sediment to hold more water than pure sand or silt; (2) clay provides more cohesive sediment interactions among particles; and, (3) the sediment depends more on interparticle forces for resistance to erosion than gravity forces. The objective of this study is to develop a single regression equation that can be used to predict the critical shear stress of either coarse or fine-grained sediments for initiation of erosion under different relative influences of widely varying resisting forces.

To accomplish this research objective, several regression models were estimated on multiple datasets obtained from the Georgia Tech laboratory erosion flume. These datasets included observations from prior studies and/or observations from this study which focused on sand-kaolinite mixtures with intermediate grain sizes in comparison to previous Georgia Tech studies. The results of the analysis integrate the findings of prior studies and predict the critical shear stress of both coarse and fine sediments as a function of percent fines, d_*, water content, clay size fraction, and the interaction between water content and clay size fraction. A weighted regression model is used to predict critical shear stress that combines the regression equation developed by Navarro and Hobson for

coarse sediments and the regression equation developed by Wang for fine sediments. The Navarro/Hobson equation uses d_* and percent fines to represent the resistance to erosion provided by the gravity force. The Wang equation uses water content, clay size fraction, and the interaction between water content and clay size fraction to represent interparticle forces of fine sediments.

This thesis integrates critical shear stress data from this study and previous studies and provides guidance into how to predict critical shear stress for erosion of both fine and coarse-grained sediments based on sediment physical parameters that can be easily measured. The proposed erosion prediction equation can be applied by measuring the sediment physical properties of a field sample and obtaining the predicted critical shear stress of that sample. Use of this equation will allow for the estimation of scour risk around bridge structures through simple geotechnical tests with no distinction being necessary between coarse and fine sediment, since this one relationship will cover both sediment erosion types.

For notational convenience, the remainder of this chapter will refer to the data from Navarro (2004) and Hobson (2008) as the "Navarro and Hobson data", and the data from Wang (2013) as the "Wang data". The terms "past studies" or "prior studies" are used to refer to the Navarro, Hobson, and/or Wang data.

5.1 Comparison with Past Research

This section compares the current study data to data from prior studies. The comparison re-estimates the Navarro Hobson and Wang equations by incorporating data from the current study or removing outliers from data of past studies. The latter part of this section compares how well these updated equations – which were independently created to predict critical shear stress for coarse-grained and fine grained sediments, respectively – predict critical shear stress across a range of both coarse and fine sediments. This comparison provides insights into the underlying causes of erosion for

different sediments and motivates the need to represent these underlying causes in a single equation.

The median particle diameter and corresponding critical shear stress are plotted in Figure 5.1 using data from the prior and current studies. This figure shows the line of the transition between fine and coarse sediments as defined by the American Geophysical Union (AGU) which is at 0.062 mm and the location of each observation in reference to that line. The majority – but not all – of the observations from this study had median particle diameters similar to those of Wang's sediments. Many of the clay size fractions (*CSF*) and percentage of fines by weight (*Fines*) from this study fell in between the values of *CSF* and *Fines* from the sediments of past studies. This is important, as the data from this study fall in the transition area between fine (cohesive) sediments and coarse (non-cohesive) sediments. Therefore, the data from this study can provide insights into how to potentially integrate prior findings for fine sediments and coarse sediments using information about clay size fractions and fines content.

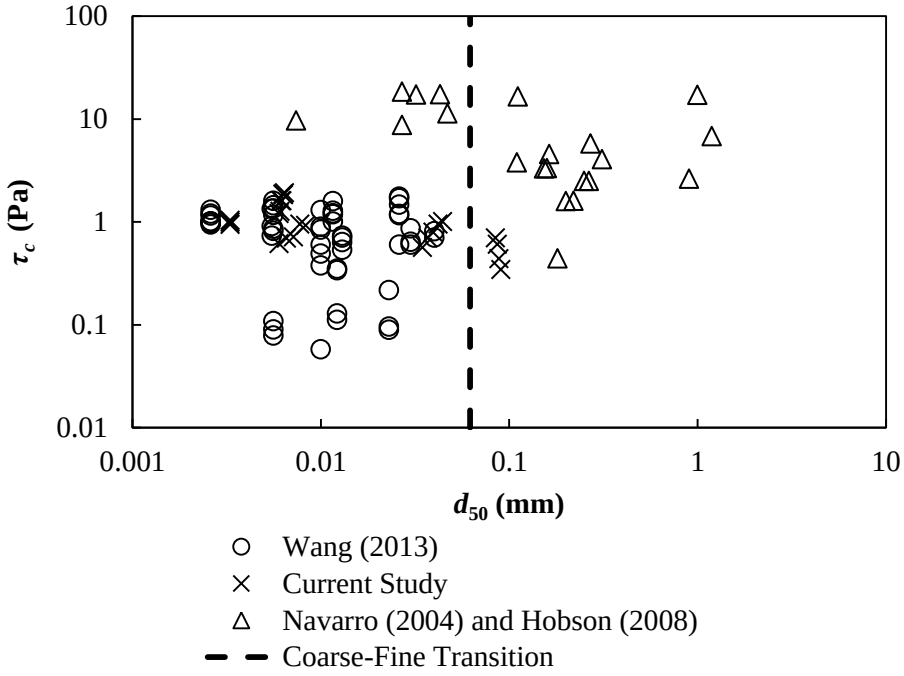

Figure 5.1: Critical shear stress and median particle diameter

This study followed experimental procedures identical to those developed in prior studies that established relationships between the Shields parameter, τ_{*c}, and specific sediment physical characteristics. Shields' parameter is a dimensionless variable used to describe incipient sediment motion, and it is defined as the ratio of applied bed shear force to the gravitational force or submerged weight acting on a sediment particle at critical conditions (Shields 1936). Shields' parameter is an important variable to characterize initiation of erosion for multiple reasons: (1) it can be used to describe both fine and coarse sediments; (2) it is a dimensionless parameter and therefore aids in the comparison of a large range of erosion thresholds; and, (3) it incorporates d_{50} which maintains the relative influence of the gravity force on sediment particles. Thus, Shields' parameter is a dimensionless variable that is useful to bridge the gap between fine and coarse sediment behavior because it incorporates both the effect of gravity and the impact

of interparticle forces on erosion resistance. Shields' parameter is defined by Eq. (2.2) and is a dimensionless form of critical shear stress. It has been related in the past to sediment physical properties such as water content, clay size fraction, percent of fines, and d_*, the dimensionless particle size (Navarro 2004, Hobson 2008, Wang 2013).

Shields (1936) used data from multiple studies to create his equation for estimating the dimensionless Shields parameter, Eq. (2.2). His equation produces a nonlinear relationship that is represented in Figure 5.2 as a solid black line. This curve represents the expected critical Shields value for a specific dimensionless diameter of pure silt or clean sands and gravels. The estimation of the Shields parameter obtained by Navarro and Hobson as a best fit of their data is given by

$$\hat{\tau}_{*_c} = 0.644 \times 10^{2.68 Fines} d_*^{-0.409} \tag{5.1}$$

Eq. (5.1) and is shown in Figure 5.2 by the dashed lines for constant values of *Fines*. The slopes of the lines from Eq. (5.1) are equal and nearly match the slope of the Shields curve in the silt size range with the lines moving upward for larger values of *Fines.* Each data point in the figure is an experimentally measured value from either the Navarro-Hobson data or the current study. The Navarro and Hobson data are shown with black diamonds and all other data points are from the current study.

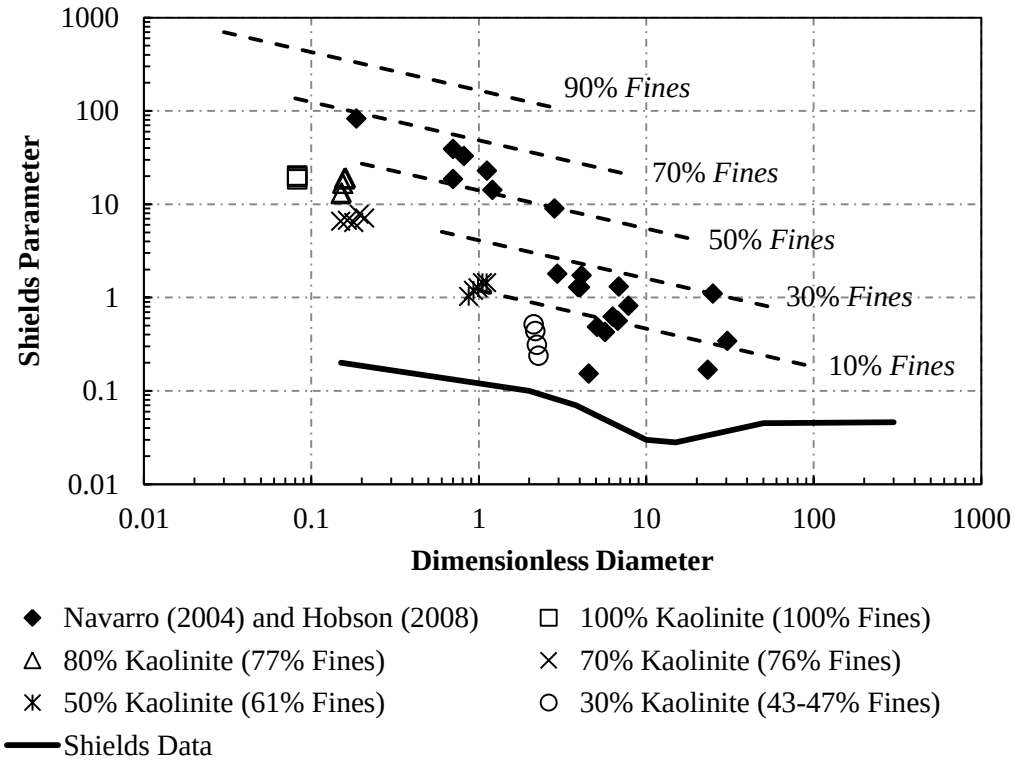

Figure 5.2: Navarro and Hobson data and equation with data from this study

Source: Adapted from Hobson (2008) Figure 4.4

The comparison in Figure 5.2 indicates that data from the current study do not directly correlate with the proposed equation from Hobson (2008). Eq. (5.1) overestimates the Shields parameters for sand-kaolinite mixtures, most likely because of their high fines concentration. This means that Eq. (5.1) provides a good estimation of coarse sediment critical shear stress but does not accurately predict critical shear stress for sediments that lie across the fine-coarse sediment dividing line. The dimensionless particle sizes of the current study's mixtures are smaller than the Navarro-Hobson sediment sizes and therefore provide a transition from the Navarro-Hobson data to the Wang data.

In order to explore this transition range, a new "baseline" Navarro-Hobson equation needed to be estimated. This modified equation was estimated after removing outliers and data points from the Navarro and Hobson data that did not have all of the necessary parameters for the full "integrated" regression model developed as part of this research. In particular, data points that did not have a water content value or a definite critical shear stress value were removed. The Navarro and Hobson equation was updated using this modified dataset and is shown as Eq. (5.2) which is very similar to the original Eq. (5.1) and has statistics for goodness of fit measures of R^2 = 0.90 and *SE* = ±0.28; these measures are identical to the goodness of fit values for Eq. (5.1).

$$\hat{\tau}_{*_c} = 0.668 \times 10^{2.51 Fines} d_*^{-0.423} \tag{5.2}$$

The Navarro-Hobson data provide a relationship between critical shear stress and sediment erodibility variables for coarser sediments, while Wang's data result in a relationship between critical shear stress and sediment erodibility for fine sediments. The current study also includes fine sediments. Wang analyzed sediment mixtures of ground silica and Georgia kaolinite which included sediments that were the same size and smaller than the current study's sand-kaolinite mixtures. Wang focused on how the water content and clay size fraction by weight, *CSF*, affect the Shields parameter and developed Eq. (5.3) to show this relationship.

$$\hat{\tau}_{*_c} = 8.46 - 27.76w + 73.69CSF + 83.22(wxCSF) \tag{5.3}$$

Her equation was generated from her data alone and had goodness of fit statistics of R^2 = 0.88 and *SE* = ±3.17. Water content (*w*) and clay size fraction (*CSF*) are both substituted into Eq. (5.3) as decimal fractions.

A comparison of the data from Wang's study and all of the data from this study is found in Figure 5.3. The equation Wang developed is shown with dotted lines for constant *CSF*. A good correlation between this study and Wang's study can be seen in the 100%, 80%, and 70% kaolinite mixtures. These mixtures acted cohesively during the erosion tests and

fall along the appropriate lines based on values of *CSF*. The 50% and 30% kaolinite mixtures do not appear to agree as well with the equation developed by Wang, most likely because they behaved more like granular, coarse sediments.

Surface erosion of cohesive sediment is characterized by detachment of small groups, or flocs, of sediment from the total sample and entering the flow of water, not the removal of individual particles. The surface erosion of clusters of kaolinite particles indicates that the structure of the sediment is a matrix composed of fine kaolinite particle structures and embedded sand grains. Erosion of small chunks, not individual kaolinite particles, occurs when the critical shear stress is overcome for the group of particles as a whole and the floc is carried downstream. This grouping of particles shows that the interparticle forces are dominating the resistance to erosion and signifies fine sediment erosion. Coarse or noncohesive sediment erosion is defined by the removal of individual sand grains from the sample mass when the gravity force is overcome by the applied bed shear stress. Individual particle erosion shows that the structure of the sediment is a sand-dominated structure and there are minimal interparticle forces resisting erosion. In this case, only the submerged weight of individual particles resists the erosion. The difference in erosion behavior between fine and coarse sediments shows the difference in sediment structure and displays the two distinct forces that are resisting the erosion.

Coarse sediment erosion behavior for the 50% and 30% kaolinite mixtures explains why their positions on Figure 5.3 do not align with the erosion estimation for cohesive sediments. Water content does not have much influence on the critical shear stress for these sediment mixtures. The fine sediment erosion behavior, on the other hand, explains why the values for 100%, 80%, and 70% kaolinite mixtures agree so well with the equation produced by Wang for kaolinite-silt mixtures.

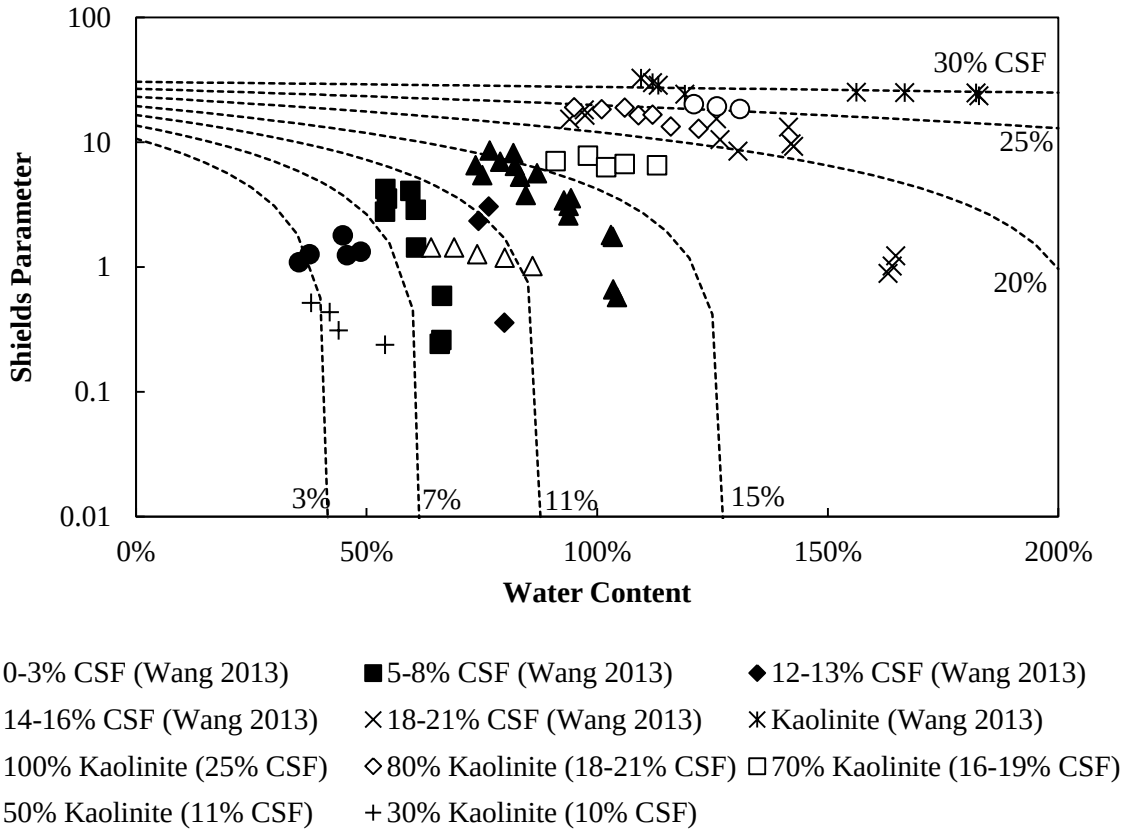

Figure 5.3: Shields' parameter vs water content for specific clay size fractions

Source: adapted from Wang (2013) Figure 5.12

Water content was used instead of bulk density as a primary factor in the estimation of the Shields parameter for Eq. (5.3) because water content is a more direct measure of the porosity of a fully saturated sediment. Fine sediments tend to have higher water contents than coarse sediments, because of the clay size fraction that has a high water content capacity and holds water in the sediment. This relationship is also shown in Table 4.3, for when kaolinite content increases, so too does water content. However, water content and clay size fraction have opposite effects on the critical shear stress. Erosion threshold, or critical shear stress, decreases as water content increases whereas an increase in clay size fraction correlates to an increase in critical shear stress. This is

shown in Eq. (5.3) by the negative sign in front of the water content parameter and the positive sign for *CSF*. These two separate influences on the critical shear stress create a balance of positive and negative contributions to the erosion threshold. This is why both water content and clay size fraction were included in the equation. The interaction term of $w \times CSF$ was included because of the interdependence of water content and clay size fraction.

To compare the data sets of Wang and the current study, a new regression equation was developed using Minitab 16 Statistical Software.

$$\hat{\tau}_{*_c} = 3.54 - 22.2w + 93.7CSF + 63.0(wxCSF) \tag{5.4}$$

The same input parameters of *w*, *CSF*, and $w \times CSF$ were used for Wang's and this study's mixtures. The developed equation, Eq. (5.4), is plotted in Figure 5.4 with constant values of fines, similar to Figure 5.3. This equation has the same form as Eq. (5.3) from Wang (2013) with identical signs before each parameter. Only a slight variation in each coefficient occurs, but with respective magnitudes remaining fairly constant. The goodness of fit statistics for this equation based on the data from the Wang study and this study are $R^2 = 0.83$ and $SE = \pm 3.617$.

In the figure are all three data sets (from Navarro and Hobson, Wang, and the current study), to display the Shields parameter predictions of each type of sediment when sorted according to the clay size fraction. Wang's data follow the curves of constant *CSF* consistently, and the cohesive data from this study agree as well, but the data from Navarro and Hobson and the coarser sediment data from this study are not as well predicted by Eq. (5.4). This shows that Wang's equation based on water content and *CSF* is most appropriate for predicting critical shear stress of cohesive sediment although it is consistent with some of the coarse sediment data. However, Wang's equation does not fit the coarser sediment data as well as the Navarro and Hobson equation as will be demonstrated subsequently.

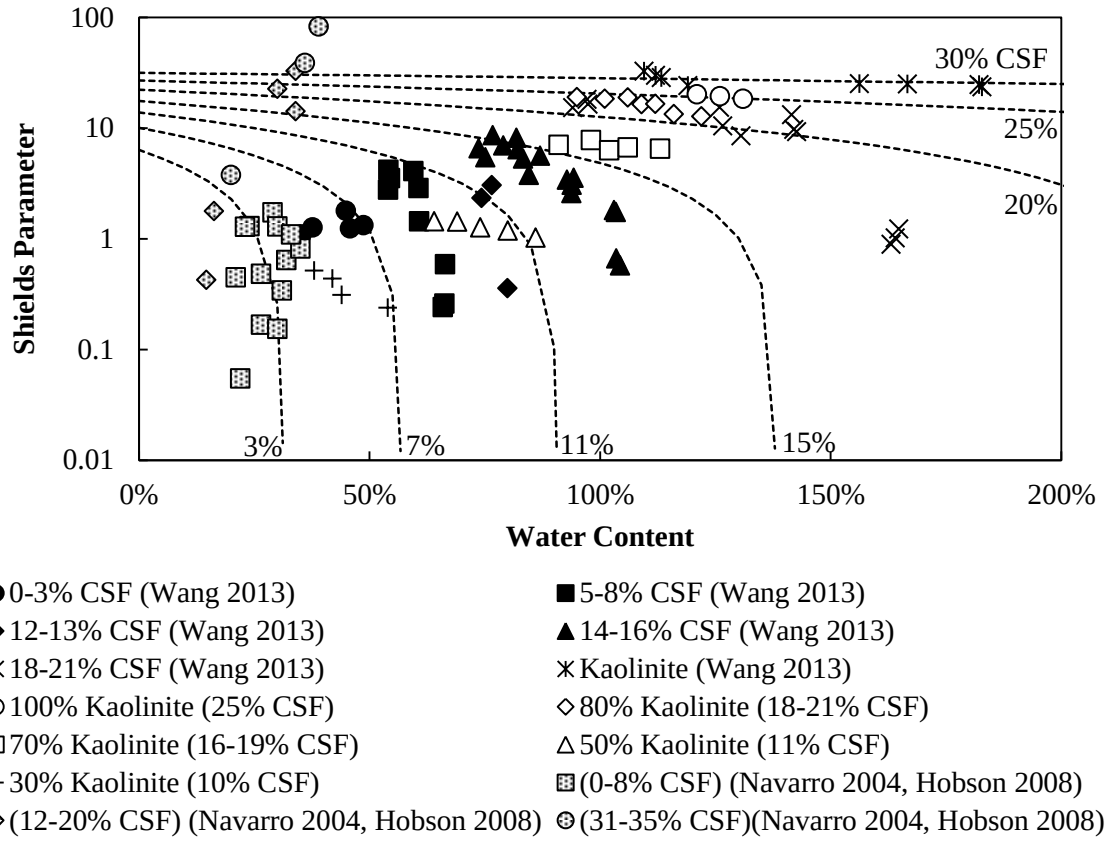

Figure 5.4: Comparison of all data sets with Eq. (5.4)

Figure 5.4 shows that Eq. (5.4) seems to fit the coarse sediment observations that have low or high amounts of *CSF*; however, the prediction accuracy is not as good for coarse sediment observations from Navarro and Hobson with *CSF* in the middle range. This suggests that at least some of the same factors that influence coarse sediment critical shear stress also affect critical shear stress for fine sediment erosion; however, additional parameters (or other parameters) may provide a better fit across all of the data points. Based on these insights, this analysis will be extended across both coarse and fine sediment critical shear stress data.

5.2 Analysis of Fine and Coarse Sediments

This section describes the regression analysis that was performed to assess the goodness of fit and prediction of different equations using data from the current and prior studies.

As discussed in the previous section, there are several sediment properties or parameters that influence erosion. Deciding which of these parameters – or set of parameters – to include in a regression model can be challenging. This decision is further complicated if these parameters will be used to estimate both fine and coarse sediment critical shear stress. With respect to estimating critical shear stress of fine sediments, water content, clay size fraction, and percent of fines by weight have been previously used in the literature (Rowell 1994, Ravisangar et al. 2001, 2005; Grabowski et al. 2001, Avnimelech et al. 2001, van Ledden et al. 2004, Thoman 2008). Water content and bulk density have both been previously demonstrated to be important factors in the erosion of fine sediments (Avnimelech et al. 2001, Ravisangar et al., 2005, Gerbersdorf et al., 2007). The clay particles within the fines content provide the cohesive properties (van Ledden et al., 2004). Median particle size is used most commonly as the dividing criterion between fine and coarse sediment but not as often in predicting erosion parameters. Sediments with similar median particle sizes, but largely different grain size distributions, can have different physical properties which lead to distinct erodibility characteristics. This is why median particle size has typically not been used in the literature, since it does not accurately represent the size distribution of the sediment.

Other studies have been performed on sediment composed of sand and fines that lie close to the transition line between fine and coarse sediments (van Ledden 2003, Van Kessel 2011, Jacobs 2011). The parameters used to quantify erosion of mixtures of fine and coarse sediment in these studies fall into three categories: (1) a representation of the size distribution; (2) a parameter to show the void space in the sediment; and, (3) a variable or group of variables to capture the cohesive behavior of the sediment. The

specific parameters used in this study to represent these three classifications are the clay size fraction, water content, fines content, and an interaction term of *w*×*CSF*. The clay size fraction and fines content taken together provide information on the size distribution of the sediment. Since sediments in these erosion tests are fully saturated, the water content is a suitable property to quantify the void space. The interaction term of water content and clay size fraction is used to characterize the cohesive behavior of the sediment. The interaction term is also included because it represents the interconnectedness of water content and clay size fraction. As *CSF* increases, water content increases too, but they have opposite effects on the critical shear stress.

The interaction term was chosen over the plasticity index to represent cohesive behavior since *CSF* is a more direct estimator of and contributor to cohesive behavior. Plasticity index is only applicable for fine, plastic sediments. Nonplastic coarse sediments cannot be represented by the plasticity index. The clay size fraction better represents the cohesiveness of both fine and coarse sediment near the transition line because both types of sediment will have a value for the *CSF*, even if it is small or zero. Furthermore, plasticity index could be viewed as a secondary variable that is positively correlated with the more fundamental variable of *CSF*.

Another parameter to include in the analysis is the dimensionless grain diameter since it incorporates the d_{50} of the sediment which is directly involved in determining the critical shear stress of coarse sediment from the Shields diagram or Eq. (5.2) while it presents a reference variable for the gravity influence, or lack thereof, for critical shear stress of fine-grained sediment. In conjunction with fines content, d_{50} also supplies information on the grain size distribution. The d_* parameter was included in the estimation equation based on the Navarro-Hobson data and therefore will be included in the regression analysis for all the data as well.

All of these parameters, *w*, *CSF*, *w*×*CSF*, *Fines*, and d_*, were used in the Minitab 16 Statistical Software to analyze a dataset that contained observations from all three

studies (i.e., the current study and the Navarro-Hobson and Wang studies). The five parameters were employed and combined in different subsets or groups, to determine which parameters best fit the data. This Minitab program uses common statistical goodness of fit values of R^2, R^2_{adj}, and *SE* but also calculates the Mallows C_p value. Mallows C_p displays the proportion of the sum of the squares of the model being evaluated, SSE_p, to the mean squared error of the model which includes all parameters, MSE_{total}. This calculation is shown below in Eq. (5.5) with *n* representing the number of data points and *p* being the number of parameters for that model.

$$C_p = \frac{SSE_p}{MSE_{totl}} - (n - 2p) \tag{5.5}$$

The fit of an equation increases as the Mallows C_p value decreases and nears the number of parameters applied. The results from the subset selection are shown below in Table 5.1.

Table 5.1: Regression statistics for sediment parameters

					Predictor Used				
Model	R^2	R^2_{adj}	Mallows C_p	*SE*	*w*	*CFS*	*Fines*	d_*	*w*×*CSF*
1	56.2	55.8	26.6	7.9217		X			
2	25.6	24.9	111.8	10.329					X
3	63.1	62.3	9.7	7.3164	X	X			
4	59	58.1	21	7.7096		X			X
5	65.5	64.4	5	7.1121	X	X			X
6	63.5	62.4	10.4	7.3074	X	X		X	
7	66.3	64.9	4.7	7.0637	X	X	X		X
8	65.5	64	7	7.1499	X	X		X	X
9	66.5	64.7	6	7.0742	X	X	X	X	X

The final equation chosen to represent all of the data is Model 7, given by Eq. (5.6).

$$\hat{\tau}_{*_c} = 1.68 - 27.1w + 97.0CSF + 72.8(w \times CSF) + 5.01Fines \quad (5.6)$$

This model was chosen due to its Mallows C_p value relative to the number of parameters used and its small value of standard error, *SE*. The Mallows C_p value is the smallest of all models and is closest to the number of parameters used in that equation. This model was chosen over Model 5 and Model 8 because it included the percent of fines by weight, *Fines*. The inclusion of this parameter introduces a representation of the size distribution when used in conjunction with the clay size fraction. From the *Fines* value of a sediment, the amount of coarse sediment particles in that sediment can be calculated and then when compared with the *CSF* the amount of silt can be inferred also as percent fines minus the percent of clay size particles. The *Fines* were chosen in preference to d_* because the dimensionless diameter is directly correlated with the *CSF* whereas the correlation between *Fines* and *CSF* is weaker. As *CSF* increases, the dimensionless diameter decreases, whereas if *CSF* increases, *Fines* may increase, decrease, or remain constant. Eq. (5.6) combines the parameters from Navarro (2004), Hobson (2008) and Wang (2013) to represent each group of data along with the data from the current study. The goodness of fit measures are R^2 = 0.663 and *SE* = ±7.06 when applied to the dataset that contains observations from current and prior studies.

The last alternative to estimate the critical shear stress for both fine and coarse sediments is to implement a weighting factor on two of the equations. Depending on the weight chosen, a fraction of one equation plus (1-this fraction) times the other equation is utilized to calculate the Shields parameter. If one equation represents the behavior of cohesive sediment and the other equation characterizes noncohesive sediment, then with the appropriate weight, each respective equation can be applied to the corresponding data. The form of this weighted equation is shown in Eq. (5.7) with the weight, *r*, applied to one equation and (1-*r*) applied to the second equation.

$$\hat{\tau}_{*c} = r \times \hat{\tau}_{*c1} + (1-r) \times \hat{\tau}_{*c2} \tag{5.7}$$

$$r = Fines^{0.235} \tag{5.8}$$

in which $\hat{\tau}_{*c1}$ is calculated from an equation based on fine sediment data and $\hat{\tau}_{*c2}$ from a corresponding equation for coarse sediment data. The two equations chosen to represent critical shear stress of fine and coarse sediments are Eq. (5.4) and Eq. (5.2), respectively. The weight, *r*, was selected to be the percent fines raised to a power, as is shown by Eq. (5.8). The *Fines* was applied as the weight because it allows for only the fine sediment critical shear stress equation to be applied when *Fines* = 100%, or for a weight of *r* = 1. For any *Fines* value less than 100%, the two equations were then applied together in varying degrees. This produced a fit to the fine sediment data very similar to that of Eq. (5.4) and then a fit for coarse sediment data using a combination of the two equations. The entire equation, Eq. (5.9), can be applied to calculate both coarse and fine sediment critical shear stress and can be compared with Eq. (5.6) and other estimates for both critical shear stress data sets.

$$\begin{aligned}\hat{\tau}_{*c} = {} & (Fines^{0.235}) \times (3.54 - 22.2w + 93.7CSF + 63.0(w \times CSF)) \\ & + (1 - Fines^{0.235}) \times (0.668 \times 10^{2.51 Fines} \times d_*^{-0.423})\end{aligned} \tag{5.9}$$

The exponent that is applied to the weighting factor was found by using the GRG nonlinear solver function in Excel 2010. The solver iterated on the exponent while minimizing the squared sum of the errors or residuals, *SSE*, and determined the exponent which when applied to the *Fines* as a weight produced the best fit equation for all data sets. The value of the exponent was calculated as 0.235 and a graphical representation of the weighting factor as a function of *Fines* is shown in Figure 5.5 for each data point in all data sets. The weighting factor was 1.0 for all of the Wang data set.

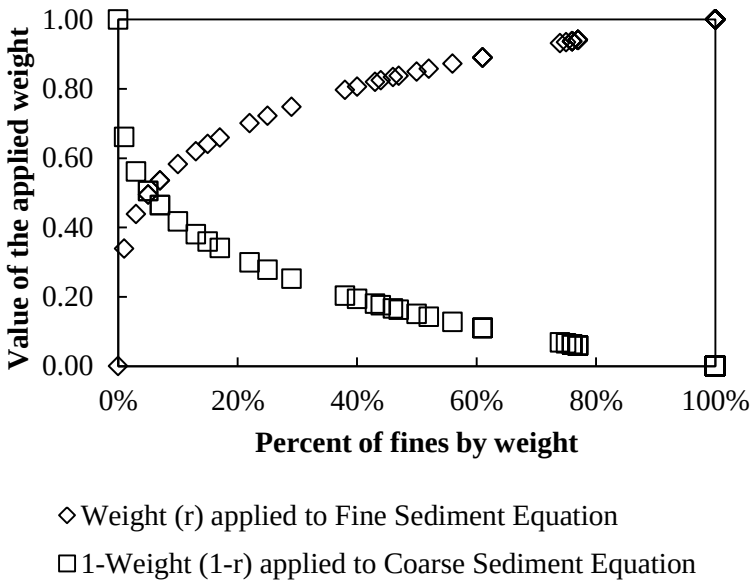

Figure 5.5: Values of the weight, *r*, and (1-*r*) for each *Fines* values in all data sets

A quick summary of all equations used to estimate critical shear stress for fine and coarse sediments can be seen in Table 5.2. These equations were applied to each data set individually and in combinations to identify which equation provided the best fit of the data. This comparison of all data sets and all equations is shown in Table 5.3.

Table 5.2: Summary of equations with data sets used

Equation Number	Equation	Data Set Used to Calculate Equation
(5.3)	$8.46 - 27.76w + 73.69CSF + 83.22(w \times CSF)$	W
(5.4)	$3.54 - 22.2w + 93.7CSF + 63.0(w \times CSF)$	W, CS
(5.2)	$0.668 \times 10^{2.51 \times Fines} \times d_*^{-0.423}$	NH
(5.6)	$1.68 - 27.1w + 97.0CSF + 72.8(w \times CSF) + 5.01Fines$	W, CS, NH
(5.9)	$(Fine^{0.235}) \times$(Eq.(5.4)) + $(1-Fines^{0.235}) \times$(Eq. (5.2))	(W, CS) & (NH)

Key: (W = Wang, CS = Current Study, NH = Navarro and Hobson)

Table 5.3: Summary of fit for each equation and each data set

Data Set Applied	Equation Applied									
	(5.3)		(5.4)		(5.2)		(5.6)		(5.9)	
Wang & Current	*SSE*	1034	*SSE*	968	*SSE*	-	*SSE*	959	*SSE*	1194
	SE	3.69	*SE*	3.57	*SE*	-	*SE*	3.55	*SE*	3.96
	R^2	0.82	R^2	0.83	R^2	-	R^2	0.83	R^2	0.79
Wang only	SSE	503	*SSE*	553	*SSE*	-	*SSE*	560	*SSE*	553
	SE	3.11	*SE*	3.26	*SE*	-	*SE*	3.28	*SE*	3.26
	R^2	0.88	R^2	0.87	R^2	-	R^2	0.87	R^2	0.87
Current only	*SSE*	531	*SSE*	415	*SSE*	-	*SSE*	399	*SSE*	641
	SE	4.91	*SE*	4.34	*SE*	-	*SE*	4.26	*SE*	5.40
	R^2	0.61	R^2	0.70	R^2	-	R^2	0.71	R^2	0.53
Navarro and Hobson	*SSE*	4181	*SSE*	3893	*SSE*	965	*SSE*	3732	*SSE*	2965
	SE	14.83	*SE*	14.31	*SE*	7.13	*SE*	14.01	*SE*	12.49
	R^2	0.48	R^2	0.51	R^2	0.88	R^2	0.53	R^2	0.63
All Data Sets	*SSE*	5209	*SSE*	4855	*SSE*	-	*SSE*	4647	*SSE*	4160
	SE	7.33	*SE*	7.07	*SE*	-	*SE*	6.92	*SE*	6.55
	R^2	0.62	R^2	0.65	R^2	-	R^2	0.66	R^2	0.70

The purpose of Table 5.3 is to show how each equation fit each respective set of data. These data represent (1) mostly coarse sediment data from the Navarro and Hobson studies; (2) fine sediment data from the Wang study; and (3) a mixture of coarse and fine sediment data from the current study. The equation derived from the Navarro and Hobson data was a realistic fit only for the Navarro and Hobson data which is why the rest of the rows for the Eq. (5.2) column are blank. The four remaining equations accurately predicted critical shear stress for Wang's data (this can be seen by the similar goodness of fit statistics across these models). This means that any of these four equations could be used to represent critical shear stress of fine sediments similar to Wang's laboratory silt and kaolinite samples.

The row that compares the goodness of fit measures for just the data from the current study shows that the regressions based on Eq. (5.4) and Eq. (5.6) provided the best fit of the data. This is not too surprising, given Eq. (5.4) represents the critical shear stress of fine sediments, and the majority of observations in the current study (20 of 24 observations) represent fine-grained sediments. Eq. (5.6), which represents erosion behavior of both coarse and fine grained sediments, slightly fits the data better. The equation that fit the current study's data the worst (excluding Eq. (5.2)) was the weighted equation.

However, the row that compares the goodness of fit measures for the Navarro and Hobson data shows that the weighted equation accurately predicts erosion behavior of coarse sediments. Excluding Eq. (5.2) (which was calibrated using only data from the Navarro and Hobson study), the weighted equation, Eq. (5.9), fits the data the best. This provides evidence that the weighting factor of $Fines^{0.235}$ can be used to represent critical shear stress for coarse-grained sediments.

Finally, the three equations that most accurately fit all data sets, Eq. (5.4), Eq. (5.6), and Eq. (5.9) are compared graphically. The weighted equation does provide the overall best fit for the "all data set" model, but since the three equations are similar in

their goodness of fit measures, it is important to see how the data are predicted. The predictions of these three equations for the Shields parameter are compared with its measured value in Figure 5.6. The first two parts, (a) and (b), of Figure 5.6 represent Eq. (5.4) and Eq. (5.6) and show that they both produce almost identical fits to all of the data sets. All three of the equations seem to produce very similar results for the Wang data, but the differences in the equations lie in the predicted values for Navarro and Hobson data and the data from the current study. This variance between the equations mimics the information seen in the statistics in Table 5.3. Eq. (5.4) and Eq. (5.6) fit the current study data the best out of the three, but the weighted equation is the best fit for the Navarro and Hobson data.

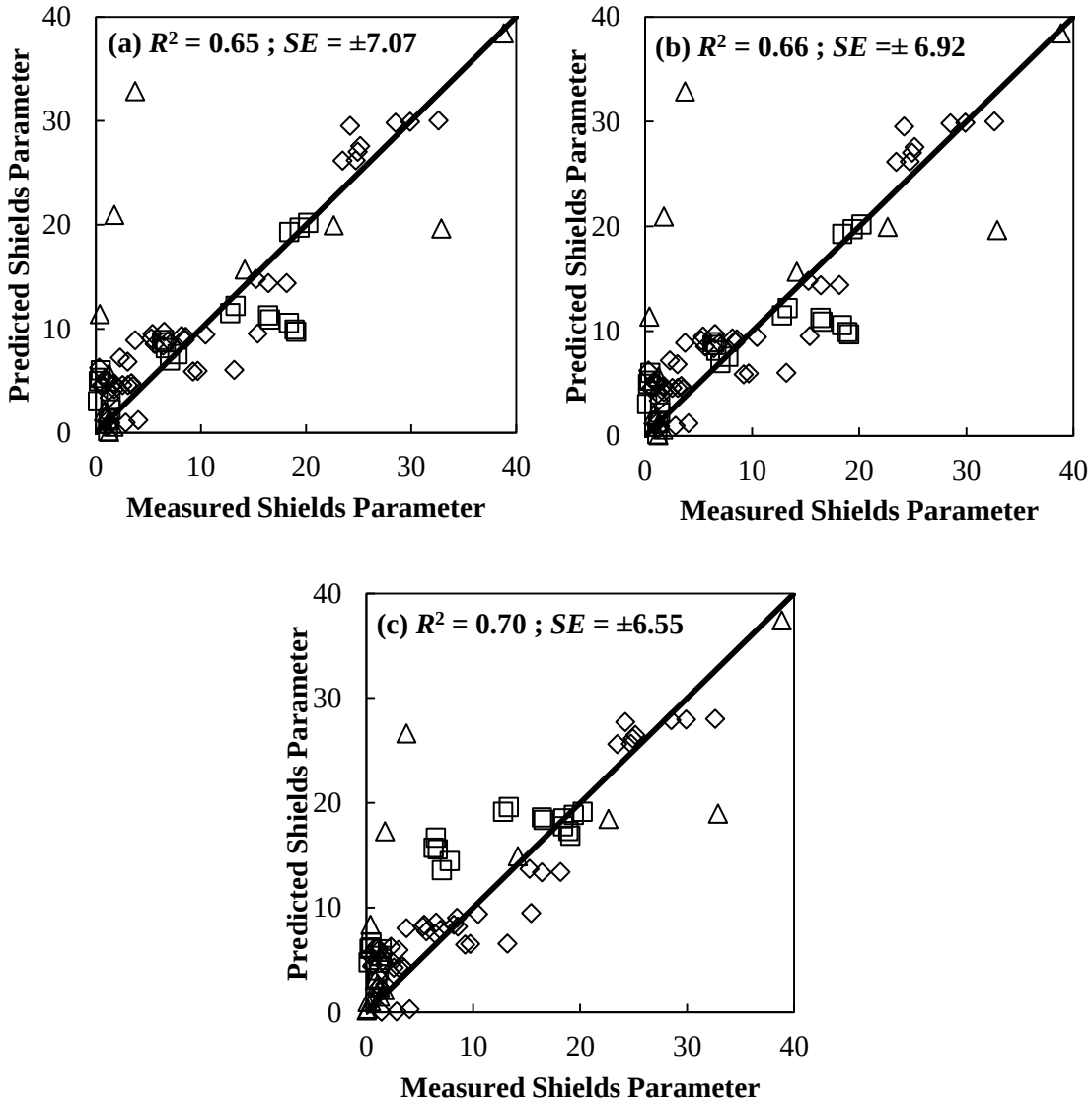

Figure 5.6: Comparison of the predictions of (a) Eq. (5.4), (b) Eq. (5.6), and (c) Eq. (5.9)

From Table 5.3 and Figure 5.6, it is shown that Eq. (5.9), the weighted equation, is the best fit of all the data as a whole. Individually it is noted that it is often the second best fit for a specific data set, since it is not a better fit than the equation derived from that data specifically. The weighted equation predicts the critical shear stress values of Wang (2013) just as well as any other applied equation. This fit to Wang's data represents the ability of Eq. (5.9) to predict fine, cohesive sediment erosion. It also shows an accurate representation of coarse noncohesive data by fitting to the data of Navarro and Hobson better than the alternatives. Where this weighted equation does not provide as good of a fit though is in predicting the Shields values for the current study's data, which contain sediment in the transition between fine and coarse behavior. Nevertheless, the fit to this study's data is considered to be adequate.

In summary, the weighted equation was chosen as the best representation of the critical shear stress of fine and coarse sediment because of how well it represents sediments on either side of the transition line from fine to coarse sediment. It is not the best critical shear stress predictor for sediments sized very close to the transition, but provides a good estimation of what this erosion should be based on accurate predictions of either the coarse or fine sediment that it most closely represents.

Before this study, the accepted method to predict critical shear stress for fine or coarse sediment was by either using an equation based on fine sediments or one for coarse sediments individually. The boundary for applying the two equations occurred at the median diameter size, d_{50}, of 0.062 mm as defined by the American Geophysical Union, with the fine sediment equation being used for smaller sediments and the coarse equation being used for larger sediments. This approach does not provide a clear enough line for which equation to use though, as is seen in Figure 5.1 for some of the Navarro-Hobson data which is well predicted by the coarse equation even though it includes some fine sediment sizes. This study has proposed a weighted equation that can be used for coarse and fine sediment together. It eliminates the need to have two separate equations.

This equation accurately fits the fine sediment erosion data and the coarse sediment erosion data independently, displaying its effectiveness in predicting the Shields parameter for sediments on both sides of the fine-coarse sediment transition line. This equation is a better alternative than using two separate equations for a few reasons; (1) it reduces the number of equations down to one and eliminates the need for a dividing criteria to specify which of the two equations to use; (2) it has proved to accurately predict both fine and coarse sediment critical shear stresses; and (3) it establishes a structure for future studies to acquire more data near the transition from fine to coarse and calibrate the equation so that it more accurately fits the sediments near the transition.

There are a few limitations to the weighted equation that incorporates two equations for fine and coarse sediment values of critical shear stress, Eq. (5.9). The weighted equation does produce some negative Shields values. This error occurs when the sediment has a very low percentage of clay which nullifies the impact of the clay in the fine sediment erosion prediction equation. Thus the water content, with its negative coefficient in the equation, then controls the erosion prediction and produces a negative predicted Shields parameter. The combined data sets include 99 data points; 54 from Wang (2013); 24 from the current study; and 21 from Navarro (2004) and Hobson (2008). Of these 99 data points, the weighted equation produces 11 negative predicted Shields values. The 88 positive values are plotted in Figure 5.6. Another limitation comes from field sample sediments that were not fully saturated. The samples had a high *CSF* but a lower water content than the typical fully saturated water content for that *CSF* value. This lower than fully saturated water content may have resulted in an over-prediction of the Shields parameter.

This weighted equation is also limited to sediments with physical properties of similar values. Table 5.4 contains the range of properties found in these data sets. The weighted equation poorly predicts sediments that are 100% silt, since only the fine sediment equation is utilized but there is no clay to counteract the negative influence of

the water content in the equation. This prediction relationship produces negative Shields parameters for 100% silt sediments, which is not realistic. Therefore, this equation is limited to sediments with either a nonzero value of clay or a nonzero value of coarse sediment.

Table 5.4: Range of physical properties in sediments from all data sets

Range	Min	Max
w	15%	183%
CSF	0%	35%
Fines	0%	100%
d_{50} (mm)	0.0026	1.19
τ_c (Pa)	0.058	18.38
τ_{*c}	0.055	82.92
d_*	0.07	30.48

5.4 Summary of Analysis and Discussion

Past studies have estimated equations to independently predict the critical shear stresses of either fine or coarse sediments. Specifically, the Navarro/Hobson and Wang equations predict critical shear stress based on differing sediment physical properties. The current study reanalyzed these two equations and produced two similar equations with updated data or a combination of past data and new data. The goodness of fit and prediction accuracy of these two updated equations were examined for various datasets (i.e., data from the Navarro and Hobson study, data from the Wang study, data from the current study, and data that combined observations from all of these prior and current studies). Based on insights from this initial analysis, a weighted equation that incorporated factors from both the Navarro/Hobson and Wang equations was proposed. The weighted equation (which used a weight of *Fines* raised to a power of 0.235) was

found to provide the best fit to the Wang data and the data of Navarro/Hobson, but did not provide the best fit for the current study's data. This weighted equation was still chosen as the best option to predict sediment critical shear stress over the transition of fine and coarse sediments though because of its accuracy for predicting erosion thresholds for fine and coarse sediments, respectively.

The weighted equation predicts the Shields parameter for a sediment based on four sediment physical properties: water content, percent of fines, clay size fraction, and the dimensionless diameter. These parameters can be attributed to primary causes of both fine and coarse sediment erosion since they represent the degree of cohesive behavior, they incorporate both the gravity force and the interparticle force, and they display the size distribution and void ratio of a sediment which are crucial in describing erosion thresholds for sediments. The proposed weighted equation aims to eliminate the need to differentiate between fine and coarse sediments based on particle size diameter or erosion behavior by incorporating the prediction of critical shear stress for both types of erosion into a single equation.

CHAPTER VI

CONCLUSION AND RECOMMENDATIONS

6.1 Summary of Report

The erodibility of fine grained sediments was investigated during this study by using mixtures of fine sand and Georgia kaolinite with varying proportions of sand to kaolinite. These mixtures were created so that they would have size ranges close to the transition of fine and coarse sediment and so that they would fall in between the sediment sizes used by past researchers. The sand-kaolinite mixtures were generated in a reproducible and systematic method to ensure that mixtures with identical ratios had similar physical properties and distributions. These mixtures were then placed in a recirculating, tilting flume to measure the erosion rates that occurred at five different shear stress values. A GRG nonlinear solver was used to find the experimental critical shear stress. The physical properties of each sediment (e.g. water content, bulk density, grain size distribution, etc.) were then related to the critical shear stress to determine relationships between these parameters and the erosional strength of the sediment mixture. The erosion data for these mixtures were found to follow the data of Wang (2013) consistently so the two datasets were combined and multiple regression analysis was completed again to further analyze the effects of each sediment property. This combined data set was then used in conjunction with the data from Navarro (2004) and Hobson (2008) to establish a link between sediments that behave cohesively and granularly. These findings are limited to the laboratory made mixtures of sand-kaolinite and silt-kaolinite as well as the field samples from Georgia bridges. This relationship, which spans the transition of erosion from coarse to fine particles, should be used to estimate the erosion of sediments with similar sizes, fine content, and physical properties.

6.2 Contributions

Prior to this study, the estimation of critical shear stress for fine or coarse sediment erosion depended on a dividing criterion that differentiated between fine and coarse sediment and determined which equation should be used for the estimation. This dividing criterion, based on d_{50}, was often not the best measure of cohesive or granular behavior in a sediment. Past researchers used these separate equations to evaluate fine and coarse sediment erosion independently. In contrast, this study presented a weighted equation that incorporates fine and coarse sediment erosion prediction equations and utilizes the sediment physical property of percent of fines to apply an appropriate weighting factor to both equations. This allows for critical shear stress of a specific type of sediment to be predicted by that respective sediment type equation and eliminates the need for a dividing criterion between two separate equations. This equation has proved to reasonably approximate the Shields parameter for fine and coarse sediments individually. The weighted equation is not the best method to estimate the critical shear stress for sediment close to the transition line from fine to coarse sediments, but this equation does provide a good foundation for future studies to build upon and more accurately fine tune the equation to fit the transition sediments.

This equation can be used in conjunction with simple geotechnical tests to classify a sediment's erodibility and the associated risk of scour around hydraulic structures. Since the equation removes the need for a separation of fine and coarse, it simplifies the process of analyzing the scour risk around a bridge's foundation and can lead to a better understanding of the effects that the obstruction to the flow, provided by the bridge piers, has on the surrounding river bed.

6.3 Recommendations for Future Research

Future work related to this study should continue to try to find relationships among critical shear stress and physical sediment properties, using both field data and

laboratory mixtures. Coarse grained laboratory mixtures that closely represent the Navarro and Hobson coarse sediment, which is correctly estimated from the weighted equation, or mixtures that are similar to the 30% kaolinite mixtures of this study should be used to further validate the use of this weighted equation. Currently all of the fine data used is from laboratory sediments and all of the coarse data is from field samples; therefore, it would be an important step to incorporate laboratory coarse samples into the analysis. Out of all of the coarse sediments, the weighted equation had the best prediction for fully saturated soils. Therefore a future study analyzing the effect of a variation in water content for identical coarse sediments would provide insight into a very important factor in erosion. As more information becomes available on each physical property and its interaction with the erodibility of a sediment, it will be possible to more accurately correlate the impacts that all properties have on the erosion threshold of both fine and coarse sediment as a collection and not only individually.

In this study, the critical shear stress was studied intensively but future studies could focus on establishing a correlation between clay composition and erosion rates. The erosion threshold is an important parameter to describe incipient sediment motion but the rate of erosion that occurs for a given bed shear stress could be just as useful in determining bridge scour and river bed stability.

APPENDIX A

ALL COLLECTED EROSION DATA

Table A.1: All erosion data from experiments

Percent of Kaolinite by weight	Erosion Rate ($kg/m^2/s$)	Shear Stress (Pa)	Water Content	Average Depth (mm)	Bulk Density (kg/m^3)	Grouping
30%	0.025	2.15	34%	58.1	1862	
30%	0.045	2.83	35%	91.0	1847	
30%	0.028	3.24	36%	53.9	1841	
30%	0.012	1.7	36%	61.0	1833	
30%	0.030	2.15	36%	38.9	1832	
30%	0.037	3.24	37%	75.5	1831	
30%	0.032	2.48	37%	95.7	1831	
30%	0.032	2.15	37%	90.5	1822	
30%	0.033	2.83	38%	64.4	1820	Group 1
30%	0.016	2.15	38%	41.0	1814	
30%	0.020	1.7	38%	77.7	1810	
30%	0.021	1.7	39%	64.5	1808	
30%	0.035	2.48	39%	73.8	1807	
30%	0.021	2.15	39%	62.4	1800	
30%	0.029	3.24	40%	37.9	1798	
30%	0.041	2.48	40%	39.9	1797	
30%	0.019	1.7	40%	50.9	1795	
30%	0.058	2.83	40%	67.2	1792	
30%	0.040	2.48	40%	40.5	1792	
30%	0.037	2.48	40%	74.8	1791	
30%	0.017	1.7	41%	63.9	1783	
30%	0.013	1.7	41%	37.6	1780	
30%	0.048	3.24	42%	51.7	1777	Group 2
30%	0.029	2.15	42%	62.2	1777	
30%	0.016	1.7	42%	53.1	1773	
30%	0.032	2.83	42%	52.0	1771	
30%	0.019	2.15	42%	22.6	1770	
30%	0.043	3.24	43%	33.8	1767	
30%	0.016	1.7	43%	48.0	1766	
30%	0.070	3.24	44%	14.6	1759	
30%	0.047	2.48	44%	55.9	1759	Group 3
30%	0.043	2.83	44%	37.0	1759	
30%	0.023	1.7	44%	22.4	1757	

30%	0.068	2.83	44%	42.2	1757	
30%	0.011	1.7	44%	33.3	1752	
30%	0.026	2.15	45%	44.6	1748	
30%	0.018	1.7	45%	35.5	1748	
30%	0.019	1.7	46%	21.7	1741	
30%	0.042	2.15	46%	46.1	1738	
30%	0.087	3.24	47%	20.3	1732	
30%	0.041	2.15	49%	15.4	1712	
30%	0.021	1.7	50%	7.0	1707	
30%	0.071	2.48	51%	33.8	1694	
30%	0.048	2.15	54%	26.2	1673	
30%	0.057	2.83	54%	13.1	1670	Group 4
30%	0.037	2.15	58%	12.2	1643	
30%	0.029	1.7	67%	20.0	1589	
30%	0.032	2.48	72%	22.9	1562	
30%	0.075	2.83	73%	14.6	1557	
50%	0.024	2.15	63%	91.7	1610	
50%	0.035	2.83	64%	116.3	1604	
50%	0.043	3.24	64%	115.5	1604	Group 1
50%	0.013	2.48	64%	68.8	1604	
50%	0.014	1.7	65%	97.6	1601	
50%	0.029	3.24	65%	87.1	1599	
50%	0.013	1.7	66%	88.1	1591	
50%	0.051	2.83	68%	56.6	1584	
50%	0.025	2.83	68%	13.8	1583	
50%	0.017	2.15	69%	75.0	1575	
50%	0.018	2.15	70%	79.1	1572	Group 2
50%	0.021	3.24	70%	77.7	1572	
50%	0.020	2.48	70%	101.4	1572	
50%	0.029	2.15	70%	92.7	1569	
50%	0.052	3.24	70%	85.5	1568	
50%	0.069	3.24	71%	57.9	1567	
50%	0.018	2.48	71%	72.3	1567	
50%	0.013	1.7	72%	82.0	1562	
50%	0.025	2.48	72%	52.0	1562	
50%	0.015	1.7	72%	73.0	1561	
50%	0.109	2.83	72%	83.0	1560	
50%	0.009	1.7	75%	52.5	1547	Group 3
50%	0.031	2.48	75%	85.4	1547	
50%	0.015	2.15	75%	63.0	1545	
50%	0.016	1.7	75%	66.7	1544	
50%	0.029	2.15	75%	64.3	1544	
50%	0.107	3.24	75%	65.1	1543	

50%	0.014	1.7	76%	55.6	1539	
50%	0.012	1.7	77%	32.9	1534	
50%	0.017	2.15	78%	51.4	1531	
50%	0.014	1.7	79%	52.0	1527	
50%	0.022	2.48	80%	50.3	1523	
50%	0.016	1.7	80%	39.8	1522	Group 4
50%	0.041	2.48	80%	67.5	1522	
50%	0.027	2.15	81%	75.1	1520	
50%	0.020	2.15	81%	38.8	1520	
50%	0.169	2.83	81%	42.5	1519	
50%	0.026	2.15	81%	46.3	1516	
50%	0.254	3.24	82%	21.3	1512	
50%	0.046	2.15	82%	15.7	1512	
50%	0.016	1.7	83%	18.9	1510	
50%	0.594	3.24	83%	37.2	1509	
50%	0.032	1.7	86%	34.3	1499	
50%	0.105	2.15	86%	21.7	1495	
50%	0.013	1.7	87%	7.8	1495	Group 5
50%	0.107	3.24	87%	29.4	1493	
50%	0.069	2.15	88%	30.8	1489	
50%	0.227	2.48	89%	40.9	1486	
50%	0.101	2.48	89%	19.3	1484	
50%	0.072	2.48	95%	20.9	1462	
70%	0.025	3.24	85%	119.0	1498	
70%	0.018	2.48	87%	134.0	1489	
70%	0.016	2.15	88%	131.8	1488	
70%	0.022	2.48	88%	111.7	1486	
70%	0.012	1.7	88%	100.7	1486	
70%	0.021	2.83	90%	118.4	1478	
70%	0.032	3.24	91%	98.7	1475	
70%	0.026	3.24	91%	93.1	1475	
70%	0.013	2.83	91%	108.5	1475	Group 1
70%	0.010	1.7	92%	80.4	1471	
70%	0.020	2.48	92%	108.1	1471	
70%	0.015	2.48	93%	113.2	1469	
70%	0.006	2.15	94%	61.2	1465	
70%	0.008	1.7	94%	105.8	1464	
70%	0.027	2.83	95%	115.6	1462	
70%	0.017	2.15	95%	99.6	1461	
70%	0.016	2.15	95%	118.1	1460	
70%	0.034	3.24	96%	74.3	1459	
70%	0.012	2.48	96%	70.1	1458	Group 2
70%	0.017	2.15	96%	111.8	1456	

70%	0.012	2.83	97%	82.9	1455	
70%	0.012	1.7	97%	56.8	1453	
70%	0.011	2.15	98%	49.6	1451	
70%	0.023	2.83	98%	99.2	1451	
70%	0.007	1.7	98%	92.0	1451	
70%	0.034	3.24	98%	64.1	1450	
70%	0.034	3.24	98%	86.1	1450	
70%	0.008	1.7	98%	104.9	1449	
70%	0.027	2.48	99%	91.1	1448	
70%	0.017	2.48	99%	82.7	1447	
70%	0.032	2.48	100%	62.8	1444	
70%	0.017	2.15	101%	88.6	1441	
70%	0.016	2.48	101%	43.6	1440	Group 3
70%	0.030	3.24	102%	50.7	1438	
70%	0.027	2.83	102%	93.2	1437	
70%	0.008	1.7	102%	89.6	1437	
70%	0.041	2.83	103%	67.4	1436	
70%	0.028	2.48	104%	53.6	1431	
70%	0.010	1.7	105%	46.6	1430	
70%	0.029	2.15	105%	66.9	1430	
70%	0.012	1.7	106%	71.8	1427	
70%	0.012	1.7	106%	12.0	1426	
70%	0.058	2.48	106%	68.6	1426	
70%	0.021	2.48	106%	15.8	1425	Group 4
70%	0.023	2.15	106%	72.0	1425	
70%	0.029	2.83	107%	69.3	1424	
70%	0.009	1.7	107%	73.8	1423	
70%	0.011	1.7	108%	49.5	1421	
70%	0.023	2.83	108%	53.9	1420	
70%	0.009	1.7	108%	25.4	1420	
70%	0.164	3.24	109%	23.2	1417	
70%	0.201	3.24	109%	18.5	1417	
70%	0.010	2.15	109%	28.9	1417	
70%	0.012	1.7	109%	36.7	1416	
70%	0.064	2.48	110%	11.6	1415	
70%	0.012	1.7	111%	23.3	1412	
70%	0.043	2.83	111%	20.6	1412	Group 5
70%	0.105	2.83	111%	33.6	1411	
70%	0.103	2.48	112%	40.1	1410	
70%	0.086	2.83	113%	26.7	1407	
70%	0.078	2.48	113%	19.7	1407	
70%	0.109	2.15	113%	33.1	1406	
70%	0.008	1.7	114%	48.2	1403	

70%	0.014	2.15	115%	9.8	1402	
70%	0.032	2.15	117%	10.4	1396	
70%	0.021	2.15	117%	36.3	1396	
70%	0.103	3.24	117%	34.2	1395	
70%	0.013	1.7	119%	25.5	1392	
80%	0.021	2.83	90%	127.3	1479	
80%	0.033	3.24	91%	142.4	1473	
80%	0.024	2.48	92%	119.3	1469	
80%	0.008	1.7	93%	136.3	1468	
80%	0.037	3.24	93%	139.0	1467	
80%	0.036	2.83	94%	126.4	1464	
80%	0.008	2.15	94%	125.5	1462	Group 1
80%	0.018	2.83	95%	131.9	1459	
80%	0.048	3.24	95%	123.9	1459	
80%	0.066	3.24	95%	123.8	1459	
80%	0.019	2.48	96%	133.1	1457	
80%	0.020	2.83	97%	106.9	1454	
80%	0.015	2.48	98%	138.6	1449	
80%	0.036	2.83	99%	106.4	1447	
80%	0.032	2.83	99%	109.9	1447	
80%	0.009	1.7	99%	120.0	1446	
80%	0.104	3.24	99%	115.2	1446	
80%	0.010	2.15	101%	130.1	1439	Group 2
80%	0.027	2.48	101%	93.2	1439	
80%	0.101	3.24	102%	102.3	1438	
80%	0.023	2.48	102%	112.8	1436	
80%	0.012	2.15	102%	109.9	1436	
80%	0.111	3.24	104%	100.5	1430	
80%	0.007	1.7	104%	98.0	1430	
80%	0.022	2.48	105%	116.4	1427	Group 3
80%	0.029	2.83	106%	85.7	1426	
80%	0.056	2.83	106%	90.4	1424	
80%	0.010	2.15	107%	130.5	1423	
80%	0.086	2.83	107%	77.4	1422	
80%	0.023	2.48	107%	77.6	1421	
80%	0.009	1.7	108%	128.1	1418	
80%	0.035	2.48	110%	87.9	1414	Group 4
80%	0.137	3.24	110%	83.8	1413	
80%	0.005	1.7	110%	71.8	1413	
80%	0.019	2.15	111%	107.9	1412	
80%	0.208	3.24	111%	75.2	1412	
80%	0.019	2.15	111%	82.7	1410	Group 5
80%	0.046	2.83	112%	55.4	1409	

80%	0.106	2.83	112%	61.0	1408	
80%	0.025	2.48	112%	98.1	1408	
80%	0.080	2.83	113%	25.2	1406	
80%	0.043	2.48	114%	56.8	1403	
80%	0.006	1.7	114%	108.3	1403	
80%	0.252	3.24	114%	68.9	1402	
80%	0.010	2.15	115%	111.2	1401	
80%	0.140	2.48	115%	62.9	1400	
80%	0.160	2.83	115%	28.8	1399	
80%	0.006	1.7	116%	45.3	1398	Group 6
80%	0.037	2.15	117%	56.6	1396	
80%	0.077	2.48	117%	34.1	1394	
80%	0.069	2.48	118%	30.0	1393	
80%	0.011	2.15	118%	81.0	1392	
80%	0.148	2.83	118%	32.5	1392	
80%	0.323	3.24	119%	32.0	1391	
80%	0.030	2.15	119%	84.5	1391	
80%	0.540	3.24	119%	35.6	1390	
80%	0.007	1.7	119%	88.7	1390	
80%	0.008	1.7	119%	23.9	1389	
80%	0.274	3.24	120%	28.4	1388	
80%	0.097	2.48	120%	69.9	1387	
80%	0.054	2.15	121%	28.2	1385	
80%	0.008	2.15	121%	61.5	1384	Group 7
80%	0.016	2.15	123%	35.1	1381	
80%	0.156	2.48	124%	31.2	1379	
80%	0.063	2.15	124%	56.7	1378	
80%	0.006	1.7	124%	72.0	1378	
80%	0.054	2.15	125%	24.9	1376	
80%	0.006	1.7	125%	55.5	1375	
80%	0.009	1.7	126%	15.6	1374	
80%	0.006	1.7	127%	40.7	1370	
100%	0.015	2.15	117%	164.0	1396	
100%	0.010	2.15	120%	147.3	1387	
100%	0.015	3.24	120%	145.1	1388	
100%	0.017	3.24	120%	110.6	1388	
100%	0.006	1.7	121%	144.1	1385	Group 1
100%	0.012	2.48	122%	150.2	1382	
100%	0.016	3.24	122%	83.5	1383	
100%	0.012	2.83	123%	131.1	1381	
100%	0.007	1.7	125%	59.6	1375	
100%	0.013	2.83	126%	111.9	1374	Group 2
100%	0.010	2.83	126%	81.4	1373	

100%	0.008	2.15	126%	67.3	1374	
100%	0.015	2.48	126%	59.1	1372	
100%	0.008	1.7	127%	134.0	1372	
100%	0.012	2.48	127%	133.9	1371	
100%	0.012	2.83	127%	63.3	1371	
100%	0.026	3.24	127%	55.3	1372	
100%	0.008	1.7	127%	43.3	1371	Group 3
100%	0.012	2.48	128%	80.0	1368	
100%	0.016	2.15	128%	43.7	1369	
100%	0.006	1.7	129%	119.2	1367	
100%	0.014	2.83	130%	27.4	1364	
100%	0.013	2.48	130%	23.3	1365	
100%	0.017	3.24	131%	30.2	1362	
100%	0.013	2.15	132%	18.4	1359	

REFERENCES

Amos, C.L., Feeney, T., Sutherland, T.F., and Luternauer, J.L. (1997). "The stability of fine grained sediments from the Fraser River delta." *Estuarine Coastal and Shelf Science*, 45 (4), 507-524.

ASTM International (American Society for Testing and Materials). (2001), "Standard test method for sieve analysis of fine and coarse aggregate." *C136-01*, West Conshohochen, Pa.

ASTM International (American Society for Testing and Materials). (2007), "Standard test method for particle-size analysis of solids." *D422-63*, West Conshohochen, Pa.

ASTM International (American Society for Testing and Materials). (2010a), "Moisture content of soil." *D2216-10*, West Conshohochen, Pa.

ASTM International (American Society for Testing and Materials). (2010b), "Standard test method for liquid limit, p. l., and plasticity index of soils." *D4318-10*, West Conshohochen, Pa.

Avnimelech, Y., Ritvo, G., Meijer, L. E., and Kochba, M. (2001). "Water content, organic carbon and dry bulk density in flooded sediments." *Aquacultural Engineering*, 25(1), 25-33.

Brindley, G.W., Kao, Chih-Chun, Harrison, J.L., Lipsicas, M., and Raythatha, R. (1986). "Relation between structural disorder and other characteristics of kaolinites and dickites." *Clays and Clay Minerals*, 34 (3), 239-249.

Bundy, W.M., Johns, W.D., and Murray, H.H. (1965). "Interrelationships of physical and chemical properties of kaolinites." *National Conference on Clays and Clay Minerals*, 26, 331-346.

Gerbersdorf, S. U., Jancke, T., and Westrich, B. (2005). "Physical-chemical and biological sediment properties determining erosion resistance of contaminated riverine sediments — temporal and vertical pattern at the Lauffen reservoir/river Neckar, Germany." *Limnologica*, 35(3), 132-144.

Gerbersdorf, S., Jancke, T., and Westrich, B. (2007). "Sediment properties for assessing the erosion risk of contaminated riverine sites. An approach to evaluate sediment properties and their covariance patterns over depth in relation to erosion resistance. First investigations in natural sediments (11 pp)." *J. Soil. Sediment.*, 7(1), 25-35.

Grabowski, R. C., Droppo, I. G., and Wharton, G. (2011). "Erodibility of cohesive sediment: The importance of sediment properties." *Earth-Sci. Rev.*, 105(3-4), 101-120.

Hanson, G. J. (1990). "Surface erodibility of earthen channels at high stresses: Part I. Open channel testing." *T. Am. Soc. Agr. Eng.*, 33(1), 127-131.

Hanson, G. J., and Simon, A. (2001). "Erodibility of cohesive streambeds in the loess area of the Midwestern USA." *Hydrological Processes*, 15(1), 23-38.

Hobson, P. M. (2008). "Rheologic and flume erosion characteristics of Georgia sediments from bridge foundations," Master Thesis, Georgia Institute of Technology, Atlanta, GA.

Hoepner, M. A. (2001). "Stability of cohesive sediments from flume and rheometer measurements," Master Thesis, Georgia Institute of Technology, Atlanta, GA.

Holtz, R. D., and Kovacs, W. D. (1981). *An Introduction of Geotechnical Engineering*, Prentice Hall, New York.

Jacobs, W., Le Hir, P., Van Kesteren, W., and Cann, P. (2011). "Erosion threshold of sand mud mixtures." *Continental Shelf Research*, 31 (2011), S14-S25.

Karmaker, T., and Dutta, S. (2011). "Erodibility of fine soil from the composite river bank of Brahmaputra in India." *Hydrol. Process*., 25(1), 104-111.

Lambe, T.W., and Whitman, R.V. (1979), *Soil Mechanics, SI Version*, John Wiley, New York.

Mehta, A. J. (1991). "Review notes on cohesive sediment erosion. In Kraus, n. C., Gingerich, K. J., and Kriebel, D. L., editors." *Coastal Sediments*, 1, 40-53.

Mehta, A. J., and Partheniades, E. (1982). "Resuspension of deposited cohesive sediment beds." *18th International Conference on Coastal Engineering, Coastal Engineering Research Council, Cape Town, South Africa*.

Mehta, A. J., Hayter, E. J., Parker, W. R., Krone, R. B., and Teeter, A. M. (1988). "Cohesive sediment transport. I: Process description " *J. Hydraul. Eng*., 115 (8), 1076-1093.

Murray, H. H. (2007). *Applied Clay Mineralogy-Occurrences, Processing and Application of Kaolinites, Bentonites, Palygorskite-sepiolite, and Common Clays*, Elsevier, Oxford, UK.

Navarro, H. R. (2004). "Flume measurements of erosion characteristics of soils at bridge foundations in Georgia," Master Thesis, Georgia Institute of Technology, Atlanta, GA.

Osman, A. M., and Thorne, C. R. (1988). "Riverbank stability analysis: I. Theory." *J. Hydraul. Eng.*, 114 (2), 134-150.

Partheniades, E. (1965). "Erosion and deposition of cohesive soil." *J. Hydraul. Eng*., 91 (1), 105-139.

Partheniades, E., (2007). "Engineering properties and hydraulic behavior of cohesive sediments." *CRC, Boca Raton*. 338.

Pruett, R. J. (2000). "Georgia kaolinite: Development of a leading industrial mineral." *Mining Engineering*, 52(10), 21.

Ranjan, G., and Rao, A. R. S. (2000). *Basic and Applied Soil Mechanics*, 2nd Ed., New Edge International Publishers, New Delhi, India.

Ravisangar, V. (2001). "The role of sediment chemistry in stability and resuspension characteristics of cohesive sediments," Ph.D. Thesis, Georgia Institute of Technology, Atlanta.

Ravisangar, V., Dennett, K. E., Sturm, T. W., and Amirtharajah, A. (2001). "Effect of sediment pH. on resuspension of kaolinite sediments." *J. Environ. Eng*., 127(6), 531- 538.

Ravisangar, V., Sturm, T. W., and Amirtharajah, A. (2005). "Influence of sediment structure on erosional strength and density of kaolinite sediment beds." *J. Hydraul. Eng.*, 131(5), 356-265.

Richardson, E. V. and Davis, S. R. (2001). "Evaluating scour at bridges." *Technical Report FWHA NHI 01-001 HEC-18*, Federal Highway Administration and National Highway Institute.

Rowell, D.L., (1994). *Soil Science: Methods and Applications*, Longman Scientific and Technical, Harlow, Essex.

Santamarina, J. C., Klein, K. A., and Fam, M. A. (2001). *Soils and Waves: Particulate Materials Behavior, Characterization and Process Monitoring*, John Wiley & Sons Ltd., New York.

Shields, A. (1936). "Applications of similarity principles and turbulence research to bedload movement." California Institute of Technology, Hydrodynamics Laboratory Publication 167, USDA, Soil Conservation Service Cooperative, Pasadena, CA.

Stone, M., Emelko, M. B., Droppo, I. G., and Silins, U. (2011). "Biostabilization and erodibility of cohesive sediment deposits in wildfire-affected streams." *Water Res.*, 45(2), 521-534.

Sturm, T. W. (2001). *Open channel hydraulics: Textbook Series in Water Resources and Environmental Engineering*, 2 Ed., McGraw Hill, New York.

Sturm, T. W., Hong, S. H., and Hobson, P. (2008). *Estimating critical shear stress of bed sediment for improved prediction of bridge contraction scour in Georgia*. Georgia DOT, Report No. FHWA-GA-08-0617, Atlanta, GA.

Sturm, T. W. (2010). *Open Channel Hydraulics*. New York: McGraw Hill.

Thoman, R.W., and Niezgoda, S.L. (2008). "Determining erodibility, critical shear stress, and allowable discharge estimates for cohesive channels: case study in the powder river basin of Wyoming." *J. of Hydraul. Eng.,* 134 (12), 1677-1687.

Torfs, H., Mitchener, H., Huysentruyt, H., and Toorman, E. (1996). "Settling and consolidation of mud/sand mixtures." *Coast. Eng*., 29(1-2), 27-45.

Van Kessel, T., Winterwerp, J.C., Van Prooijen, B., Van Ledden, M., and Borst, W. (2011). "Modeling the seasonal dynamics of SPM with a simple algorithm for the buffering of fines in a sandy seabed." *Cont. Shelf Res.*, 31(10), S124-S134.

Van Ledden M. (2003). "Sand-mud segregation in estuaries and tidal basins," PhD Dissertation, Delft Univ. of Technol., Delft, Netherlands.

Van Ledden, M., van Kesteren, W. G. M., and Winterwerp, J. C. (2004). "A conceptual framework for the erosion behavior of sand-mud mixtures." *Cont. Shelf Res.*, 24(1), 1-11.

Velde, B. (1995). *Origin and Mineralogy of Clays,* Springer, New York.

Walder, J. (2015). " Dimensionless erosion laws for cohesive sediment." *J. of Hydraul. Eng.*, 10.1061/(ASCE)HY.1943-7900.0001068 , 04015047.

Wang, Y. (2013). "Effects of Physical Properties and Rheological Characteristics on Critical Shear Stress of Fine Sediments." Ph.D. Thesis, Georgia Institute of Technology, Atlanta, GA, United States.

Whitlow, R. (2001). *Basic Soil Mechanics*, Harlow, Essex, U.K.

Winterwerp, J. C., and van Kesteren, W. G. M. (2004). *Introduction to the Physics of Cohesive Sediment in the Marine Environment*, Elsevier, Amsterdam.

Winterwerp, J. C., van Kesteren, W. G. M., van Prooijen, B., and Jacobs, W. (2012). "A conceptual framework for shear flow-induced erosion of soft cohesive sediment beds." *J. Geophys. Res. Oceans*, 117(C10), C10020.